Boundary versus bulk behavior of time-dependent correlation functions in one-dimensional quantum systems

Eliëns, I.S.; Ramos, F.B.; Xavier, J.C.; Pereira, R.G.

Link to publication

Boundary versus bulk behavior of time-dependent correlation functions in one-dimensional quantum systems

I. S. Eliëns,[1,][*] F. B. Ramos,[2] J. C. Xavier,[2] and R. G. Pereira[3]

[1]*Institute for Theoretical Physics, Institute of Physics (IoP), University of Amsterdam, Science Park 904,*
1098 XH Amsterdam, The Netherlands

[2]*Universidade Federal de Uberlândia, Instituto de Física, C.P. 593, 38400-902 Uberlândia, MG, Brazil*

[3]*Instituto de Física de São Carlos, Universidade de São Paulo, C.P. 369, São Carlos, SP, 13560-970, Brazil*

We study the influence of reflective boundaries on time-dependent responses of one-dimensional quantum fluids at zero temperature beyond the low-energy approximation. Our analysis is based on an extension of effective mobile impurity models for nonlinear Luttinger liquids to the case of open boundary conditions. For integrable models, we show that boundary autocorrelations oscillate as a function of time with the same frequency as the corresponding bulk autocorrelations. This frequency can be identified as the band edge of elementary excitations. The amplitude of the oscillations decays as a power law with distinct exponents at the boundary and in the bulk, but boundary and bulk exponents are determined by the same coupling constant in the mobile impurity model. For nonintegrable models, we argue that the power-law decay of the oscillations is generic for autocorrelations in the bulk, but turns into an exponential decay at the boundary. Moreover, there is in general a nonuniversal shift of the boundary frequency in comparison with the band edge of bulk excitations. The predictions of our effective field theory are compared with numerical results obtained by time-dependent density matrix renormalization group (tDMRG) for both integrable and nonintegrable critical spin-S chains with $S = 1/2$, 1, and 3/2.

I. INTRODUCTION

Striking properties in many-body quantum systems often emerge from the interplay between interactions and a constrained geometry. In a Fermi gas confined to a single spatial dimension, for example, interactions lead to dramatically different spectral properties as compared to its higher dimensional counterparts described by Fermi liquid theory [1–4].

The low-energy limit of one-dimensional (1D) Fermi gases is conventionally treated within the Luttinger liquid (LL) framework [5]. Indispensable in this respect is the exactly solvable Tomonaga-Luttinger (TL) model [6,7], which allows a nonperturbative treatment of interactions at the cost of an artificially linearized dispersion relation for the constituent fermions. Using the technique of bosonization, the model is solved in terms of bosonic collective modes corresponding to quantized waves of density.

Static correlations and many thermodynamic properties are captured remarkably well by the Luttinger liquid approach. For many dynamic effects, however, it is clear that band curvature needs to be taken into account. For example, the relaxation of the bosonic sound modes, or the related width of the dynamical structure factor (DSF), are not captured by Luttinger liquid theory, which predicts a delta-function peak for the DSF. Attempts to treat the DSF broadening in the bosonized theory, in which the dispersion curvature translates to interactions between the modes diagonalizing the TL model, are hindered by on-shell divergences in the perturbative expansion. Certain aspects of the DSF broadening can nevertheless be captured in the bosonic basis [8–12]. An alternative approach uses a reformulation of the TL model including a quadratic correction to the dispersion in terms of fermionic quasiparticles. In the

low-energy limit, these turn out to be weakly interacting [13–15] restoring some of the elements of Fermi liquid theory in one dimension. At high energies, insight into dynamic response functions such as the DSF and the spectral function, and in particular into the characteristic threshold singularities, can be obtained by mapping the problem to a mobile impurity Hamiltonian. This approach hinges on the observation that the thresholds correspond to configurations of a high-energy hole or particle, which can effectively be considered as separated from the low-energy subband, and that the threshold singularities emerge from the scattering of the modes at the Fermi level on this impurity mode. This identifies the anomalous correlation structure of 1D gases as an example of Anderson's orthogonality catastrophe [16] and links it to the physics of the x-ray edge singularity [17]. Many new results on dynamic correlations, in general and for specific models, have been obtained this way [14,18–29]. This bears relevance to, e.g., Coulomb drag experiments [9,30–34] as well as relaxation and transport [35–39]. Dispersion nonlinearity also greatly influences the propagation of a density bump or dip, which would retain its shape when time-evolved under the linear theory but relaxes by emitting shock waves in the nonlinear theory [40–42]. Closer to the present work is the late-time dependence of correlations [43–45], which are related to the singularities in the frequency domain. Collectively, the extensions of LL theory that include band curvature effects may be called nonlinear Luttinger liquid (nLL) theory, but we will mainly be concerned with the mobile impurity approach to correlations (see Ref. [46] for further details).

Motivated by these theoretical advances, we study the effect of reflective boundaries on a 1D gas beyond the low-energy regime. Our work is also inspired by studies of "boundary critical phenomena" [47–49] within the LL framework that have unveiled remarkable effects, e.g., in the conductance of quantum wires [50–52], screening of magnetic impurities [53],

―――――
[*]i.s.eliens@uva.nl

Friedel oscillations in charge and spin densities [54–56], and oscillations in the entanglement entropy [57,58].

We focus on response functions which can be locally addressed—such as the local density of states (LDOS) and autocorrelation functions—as these are expected to show the clearest bulk versus boundary contrast. Many studies have addressed the LDOS for LLs with a boundary [59–68]. LL theory predicts a characteristic power-law suppression (for repulsive interactions) of the LDOS at the Fermi level with different bulk and boundary exponents which are nontrivially but universally related [69,70]. This has been verified using different techniques [59,60,66,71] and is used as a consistency check in the experimental identification of LL physics [72,73].

Away from the Fermi level, no universal results are known. This pertains both to general statements on the restricted energy range where the power-law scaling is valid [60,66] and to details of the line shape at higher energies. Here, we deal with the latter and argue that the nonanalyticities of, e.g., the LDOS away from zero energy can be understood in the framework of nLL theory for systems with open and periodic boundary conditions alike. The main application of our theory is in describing the power-law decay of autocorrelation functions in real time. We show that bulk and boundary exponents are governed by the same parameters in the mobile impurity model and obey relations that depend only on the Luttinger parameter. These relations provide a quantitative test of the nLL theory. We perform this test by analyzing time-dependent density matrix renormalization group (tDMRG) [74,75] results for spin autocorrelations of critical spin chains. The statement about boundary exponents applies to integrable models in which the nonanalytic behavior at finite energies is not susceptible to broadening due to three-body scattering processes [14,24]. The effects of integrability breaking are also investigated, both numerically and from the perspective of the mobile impurity model. We find that for nonintegrable models the finite-energy singularities in boundary autocorrelations are broadened by decay processes associated with boundary operators in the mobile impurity model. As a result, the boundary autocorrelation decays exponentially in time in the nonintegrable case.

The paper is organized as follows. In Sec. II, we discuss the LDOS for spinless fermions as a first example of how dynamical correlations in the vicinity of an open boundary differ from the result in the bulk. In Sec. III, we present the mobile impurity model used to calculate the exponents in the LDOS near the boundary. In Sec. IV, we generalize our approach to predict relations between bulk and boundary exponents of other dynamical correlation functions, including the case of spinful fermions. Section V addresses the question whether finite-energy singularities exist in nonintegrable models. Our numerical results for the time decay of spin autocorrelation functions are presented in Sec. VI. Finally, we offer some concluding remarks in Sec. VII.

II. GREEN'S FUNCTION FOR SPINLESS FERMIONS

We are interested in 1D systems on a half-line, where we impose the boundary condition that all physical operators vanish at $x = 0$. Let us first discuss the case of spinless fermions on a lattice. We define the (non-time-ordered)

Green's function at position x as

$$G(t,x) = \langle \{ \Psi(x,t), \Psi^\dagger(x,0) \} \rangle, \tag{1}$$

where $\Psi(x)$ annihilates a spinless fermion at position x and the time evolution $\Psi(x,t) = e^{iHt} \Psi(x) e^{-iHt}$ is governed by a local Hamiltonian H. The brackets $\langle \ldots \rangle$ denote the expectation value in the ground state of H. The Fourier transform to the frequency domain yields the LDOS

$$\rho(\omega,x) = \frac{1}{2\pi} \int_{-\infty}^{\infty} dt \, e^{i\omega t} G(t,x). \tag{2}$$

The boundary case corresponds to the result for $x = a$, where a is the lattice spacing for lattice models or the short-distance cutoff for continuum models. We refer to the bulk case of $G(t,x)$ as the regime $x \gg a$ and $vt < x$, where v is the velocity that sets the light cone for propagation of correlations in the many-body system [76]. The latter condition allows one to neglect the effects of reflection at the boundary, and is routinely employed in numerical simulations aimed at capturing the long-time behavior in the thermodynamic limit [22,24,45,77].

As our point of departure, consider the free fermion model

$$H_0 = -\frac{1}{2} \sum_{x \geqslant 1} [\Psi^\dagger(x) \Psi(x+1) + \text{H.c.}]$$

$$= \sum_k \varepsilon_k \Psi_k^\dagger \Psi_k, \tag{3}$$

where $\varepsilon_k = -\cos k$, with $k \in (0,\pi)$, is the free fermion dispersion and we set $a = 1$. The single-particle eigenstates of H_0 are created by

$$\Psi_k^\dagger = \sqrt{\frac{2}{\pi}} \sum_{x \geqslant 1} \sin(kx) \Psi^\dagger(x). \tag{4}$$

We focus on the case of half filling, in which the ground state is constructed by occupying all states with $0 < k < \pi/2$. In this case particle-hole symmetry rules out Friedel oscillations [56] and the average density is homogeneous, $\langle \Psi^\dagger(x)\Psi(x)\rangle = 1/2$. The Green's function is given exactly by

$$G_0(t,x) = \frac{4}{\pi} \int_0^{\pi/2} dk \, \sin^2(kx) \cos(\varepsilon_k t), \tag{5}$$

and the LDOS is

$$\rho_0(\omega,x) = \frac{2 \sin^2[x \arccos(\omega/\epsilon_0)]}{\pi \sqrt{\epsilon_0^2 - \omega^2}} \theta(\epsilon_0 - |\omega|), \tag{6}$$

where $\epsilon_0 \equiv |\varepsilon_{k=0}| = 1$.

The result for $G_0(t,x)$ is depicted in Fig. 1(a). First we note that, for any fixed position x, there is a clear change of behavior at the time scale $t \sim T_{\text{refl}}(x) = 2x/v$ (where $v = 1$ for free fermions). This corresponds to the time for the light cone centered at x to reflect at the boundary and return to x. For $t < T_{\text{refl}}(x)$, $G_0(t,x)$ is independent of x (i.e., translationally invariant for fixed t and $x > vt/2$) and the result is representative of the bulk autocorrelation. The arrival of the boundary-reflected correlations makes $G_0(t,x)$ deviate from the bulk case and become x-dependent for $t > T_{\text{refl}}(x)$. After we take the Fourier transform to the frequency domain,
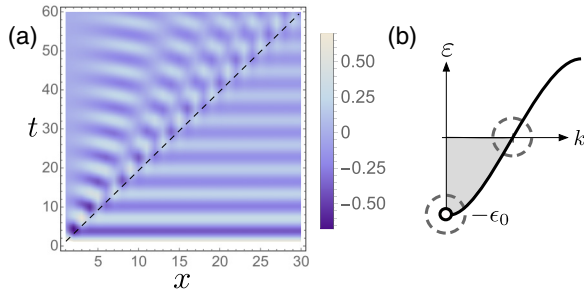
FIG. 1. (a) Green's function $G_0(t,x)$ for free fermions in a semi-infinite chain at half-filling [Eq. (5)], where x is the distance from the boundary. The dashed line represents the reflection time $T_{\text{refl}}(x) = 2x/v$ with $v = 1$. (b) The deep hole configuration responsible for the oscillations at $x = 0$ related to the singularities of the LDOS (Fig. 2). There is an equivalent high-energy particle configuration, not depicted. The dashed circles indicate the projection onto low-energy and impurity subbands important once interactions are taken into account.

the reflection time scale implies that the LDOS in Eq. (6) oscillates with period $\Delta\omega(x) \sim 2\pi/T_{\text{refl}}(x) = \pi v/x$. In the bulk case, the rapid oscillations in the frequency dependence of $\rho_0(\omega, x \gg 1)$ are averaged out by any finite frequency resolution [68]. In numerical simulations of time evolution in the bulk, the usual procedure is to stop the simulation at $t < x/v$ (or before in case the maximum time is limited by various sources of error [74,75]). This avoids the reflection at the boundary but at the same time sets the finite frequency resolution.

Let us now discuss the time dependence of the Green's function at the boundary ($x = 1$) versus in the bulk ($x \gg 1$, $vt < x$). In both cases (see Fig. 2), the Green's function shows oscillations in the long-time decay, which are not predicted by the usual low-energy approximation of linearizing the dispersion about $k_F = \pi/2$ [5]. The explanation for the real-time oscillations is the same for open or periodic boundary conditions; for the case of periodic boundary conditions, see the reviews in Refs. [43,46]. The oscillations stem from a saddle point contribution to the integral in Eq. (5) with $k \approx 0$
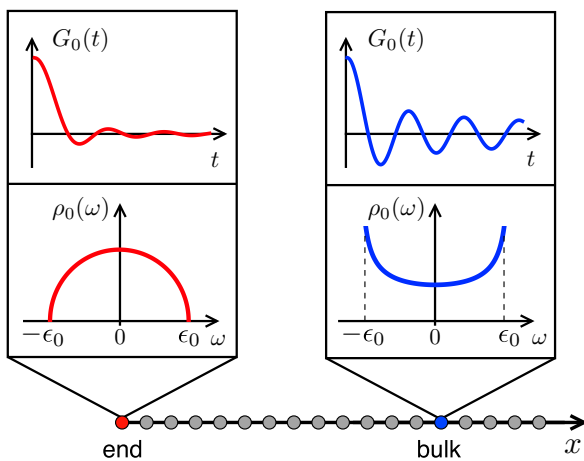

FIG. 2. Noninteracting Green's function $G_0(t,x)$ and LDOS $\rho_0(\omega,x)$. The curves on the left correspond to the chain end ($x = 1$), and the curves on the right to a site in the bulk ($x \gg 1$).

[in the hole term of $G_0(t,x)$] or $k \approx \pi$ (in the particle term). This contribution is associated with an excitation with energy ϵ_0, the maximum energy of a single-hole or single-particle excitation [see Fig. 1(b)]. We call this energy the band edge of the free fermion dispersion. The propagator of the band edge mode decays more slowly in time due to its vanishing group velocity. The importance of this finite-energy contribution is manifested in the LDOS as a power-law singularity at $\omega = \pm\epsilon_0$ (see Fig. 2). Notice the clear difference between the bulk and the boundary case: while in the bulk the LDOS has a van Hove singularity at the band edge, $\rho_0(\omega, x \gg 1) \sim |\omega \pm \epsilon_0|^{-1/2}$, at the boundary one finds a square-root cusp $\rho_0(\omega, x = 1) \sim |\omega \pm \epsilon_0|^{1/2}$.

One of the main achievements of the nLL theory is to incorporate the contributions of finite-energy excitations in dynamical correlation functions for interacting 1D systems with band curvature [43,46]. Our purpose here is to generalize this approach to describe the dynamics in the vicinity of a boundary. For concreteness, we consider the model

$$H = H_0 + V \sum_{x \geqslant 1} n(x)n(x + 1), \qquad (7)$$

where $n(x) \equiv \Psi^\dagger(x)\Psi(x)$ is the density operator and we focus on the repulsive regime $V > 0$. Importantly, the model in Eq. (7) is integrable and exactly solvable by Bethe ansatz [78]. This guarantees that the band edge of elementary excitations is still well defined in the interacting case. We postpone a detailed discussion about integrability-breaking effects to Sec. V.

Before outlining the derivation of the results for the interacting model (see Sec. III), we summarize some known results together with our findings for the Green's function and LDOS. The calculation within the LL framework leads to the well-known predictions [50,69,70]

$$G_{\text{LL}}(t,x) \sim 1/t^{\alpha+1}, \qquad (8)$$

$$\rho(\omega \approx 0,x) \sim |\omega|^\alpha, \qquad (9)$$

where the exponent α is different for x in the bulk than at the boundary (subscript "end"): $\alpha_{\text{bulk}} = (K + K^{-1})/2 - 1$ and $\alpha_{\text{end}} = K^{-1} - 1$, where K is the Luttinger parameter ($K = 1$ for free fermions and $K < 1$ for repulsive interactions). As mentioned above, the real-time oscillations are not predicted by LL theory. It is known that taking into account the finite-energy contributions within the nLL theory leads to the following contributions from the band-edge excitation in the bulk:

$$G_{\text{osc}}(t,x \gg 1) \sim e^{\pm i\epsilon t}/t^{\bar{\alpha}_{\text{bulk}}+1}, \qquad (10)$$

$$\rho(\omega \approx \pm\epsilon,x \gg 1) \sim |\omega \mp \epsilon|^{\bar{\alpha}_{\text{bulk}}}, \qquad (11)$$

where ϵ is the renormalized band edge in the interacting system and the bulk exponent for the oscillating contribution is

$$\bar{\alpha}_{\text{bulk}} = -1/2 + \gamma^2/(2\pi^2 K), \qquad (12)$$

with γ the phase shift of low-energy modes due to scattering off the high-energy hole [for free fermions, $\gamma = 0$; the phase shift for the interacting model in Eq. (7) will be specified in Sec. III].

Our new result is that the oscillating contribution at the boundary is given by

$$G_{\mathrm{osc}}(t,x = 1) \sim e^{\pm i\epsilon t}/t^{\bar{\alpha}_{\mathrm{end}}+1}, \tag{13}$$

$$\rho(\omega \approx \pm\epsilon, x = 1) \sim |\omega \mp \epsilon|^{\bar{\alpha}_{\mathrm{end}}}, \tag{14}$$

with the same band-edge frequency ϵ as in the bulk, but with a different exponent

$$\bar{\alpha}_{\mathrm{end}} = 1/2 + \gamma^2/(\pi^2 K). \tag{15}$$

When the band-edge mode is the dominant finite-energy contribution to the Green's function, the asymptotic long-time decay of $G(t,x)$ is well described by a linear combination of the Luttinger liquid term in Eq. (8) and the oscillating term in Eq. (10) or Eq. (13).

There are two noteworthy modifications in going from the bulk to the boundary: (*i*) an extra factor of $1/t$ in the decay of $G_{\mathrm{osc}}(t,x)$; (*ii*) the doubling of the $\mathcal{O}(\gamma^2)$ orthogonality catastrophe correction to the exponent [5,16]. Both are recurrent in the exponents that will be discussed in Sec. IV. Furthermore, while both exponents vary with interactions, Eqs. (12) and (15) imply the relation

$$\bar{\alpha}_{\mathrm{end}} - 2\bar{\alpha}_{\mathrm{bulk}} = 3/2, \tag{16}$$

which is independent of the nonuniversal phase shift γ.

III. MOBILE IMPURITY MODEL WITH OPEN BOUNDARY

To derive the results above, we use the mode expansion that includes band-edge excitations

$$\Psi(x) \sim e^{ik_F x}\psi_R(x) + e^{-ik_F x}\psi_L(x) + d^{\dagger}(x), \tag{17}$$

where $\psi_{R,L}$ denote the low-energy modes, $d^{\dagger}$ creates a hole in the bottom of the band ($k \approx 0$), and all fields on the right-hand side are slowly varying on the scale of the short-distance cutoff a.

A crucial assumption implicit in Eq. (17) is that we identify the excitations governing the long-time decay in the interacting model as being "adiabatically connected" with those in the noninteracting case, in the sense that they carry the same quantum numbers and their dispersion relations vary smoothly as a function of interaction strength. This condition can be verified explicitly for integrable models, where one computes exact dispersion relations for the elementary excitations. We should also note that for lattice models such as Eq. (7) the mode expansion must include a high-energy particle at the top of the band, with $k \approx \pi$ [22]. In the particle-hole symmetric case, the latter yields a contribution equivalent to that of the deep hole with $k \approx 0$, and we get the particle contribution in the LDOS simply by taking $\omega \to -\omega$ in the result for the hole contribution. More generally, the high-energy spectrum of the interacting model may include other particles and bound states, which can also be incorporated in the mobile impurity model [24]; we shall address this question in Sec. VI B.

In Eq. (17), we deliberately write the right and left movers separately, even though they are coupled by the boundary conditions [52,53]. The condition $\Psi(0) = 0$ is satisfied if we impose

$$\psi_L(0) = -\psi_R(0), \quad d(0) = 0. \tag{18}$$

These relations can be checked straightforwardly in the noninteracting case using the single-particle modes Ψ_k. The boundary condition on $d(x)$ means that for any boundary operator that involves the high-energy mode, we must take $d(a) \sim a\partial_x d(0)$.

We bosonize the low-energy modes with the conventions

$$\psi_{R,L} \sim e^{-i\sqrt{2\pi}\phi_{R,L}}, \tag{19}$$

$$\psi_{R,L}^{\dagger}\psi_{R,L} \sim \mp\frac{1}{\sqrt{2\pi}}\partial_x\phi_{R,L}, \tag{20}$$

where $\phi_{R,L}(x)$ are chiral bosonic fields that obey $[\partial_x\phi_{R,L}(x),\phi_{R,L}(x')] = \pm i\delta(x - x')$. A convenient way to treat the boundary conditions for the low-energy modes is to use the folding trick [51,52]: we include negative coordinates $x < 0$ and identify

$$\psi_L(x) \equiv -\psi_R(-x). \tag{21}$$

For the bosonic fields, we use

$$\phi_L(x) \equiv \phi_R(-x) + \sqrt{\pi/2}. \tag{22}$$

The effective Hamiltonian that describes the interaction between the band-edge mode and the low-energy modes is the mobile impurity model

$$H_{\mathrm{MIM}} = \int_{-\infty}^{\infty} dx\, \frac{v}{2}(\partial_x\varphi)^2 + \int_0^{\infty} dx\, d^{\dagger}\left(\epsilon + \frac{\partial_x^2}{2M}\right)d$$
$$+ \frac{v\gamma}{\sqrt{2\pi K}}\int_0^{\infty} dx\, d^{\dagger}d[\partial_x\varphi(x) + \partial_x\varphi(-x)]. \tag{23}$$

Here, $\varphi(x)$ is the chiral boson that diagonalizes the Luttinger model on the unfolded line

$$\varphi(x) = \frac{K^{-\frac{1}{2}} + K^{\frac{1}{2}}}{2}\phi_R(x) + \frac{K^{-\frac{1}{2}} - K^{\frac{1}{2}}}{2}\phi_R(-x), \tag{24}$$

which obeys $[\partial_x\varphi(x),\varphi(x')] = i\,\mathrm{sgn}(x)\delta(x - x')$. The parameters ϵ, $-M$ and γ are nonuniversal properties of the hole with $k = 0$ (which is treated as a mobile impurity): its finite energy cost, effective mass and dimensionless coupling to the low-energy modes, respectively. Note that the linear term in the dispersion vanishes for the band-edge mode, which is why we have to take into account the effective mass [see Fig. 1(b)]. In models solvable by Bethe ansatz, ϵ and M are determined by the exact dispersion of single-hole excitations. The coupling γ can be obtained from the so-called shift function [23,79] and the finite size spectrum [24] for periodic boundary conditions. In Galilean-invariant systems, we can relate γ to the exact spectrum by using phenomenological relations [25].

The Hamiltonian in Eq. (23) contains only marginal operators. It can be obtained from the mobile impurity model in the bulk [15] by applying the folding trick. Remarkably, all boundary operators that perturb this Hamiltonian and couple the d field to the bosonic modes are highly irrelevant, as they necessarily involve the derivative $\partial_x d(0)$ (which by itself has scaling dimension 3/2). For the moment, we neglect the effect of all formally irrelevant boundary operators, but return to this point in Sec. V.

Like in the bulk case, we can decouple the impurity mode by the unitary transformation

$$U = \exp\left\{ i \frac{\gamma}{\sqrt{2\pi K}} \int_0^\infty dx \, [\varphi(x) + \varphi(-x)] d^\dagger d \right\}. \quad (25)$$

The fields transform as

$$\tilde{\varphi}(x) = U\varphi(x)U^\dagger = \varphi(x) + \frac{\gamma}{2\sqrt{2\pi K}} F_d(x), \quad (26)$$

$$\tilde{d}(x) = Ud(x)U^\dagger = d(x)e^{-i\frac{\gamma}{\sqrt{2\pi K}}[\varphi(x)+\varphi(-x)]}, \quad (27)$$

where

$$F_d(x) = \int_0^\infty dy \, [\text{sgn}(x-y) + \text{sgn}(x+y)] d^\dagger(y) d(y). \quad (28)$$

Equation (26) implies

$$\partial_x \tilde{\varphi}(x) = \partial_x \varphi(x) + \frac{\gamma}{\sqrt{2\pi K}} d^\dagger(x) d(x). \quad (29)$$

The Hamiltonian becomes noninteracting when written in terms of the transformed fields

$$H_{\text{MIM}} = \int_{-\infty}^\infty dx \, \frac{v}{2}(\partial_x\tilde{\varphi})^2 + \int_0^\infty dx \, \tilde{d}^\dagger\left(\epsilon + \frac{\partial_x^2}{2M}\right)\tilde{d}. \quad (30)$$

The crucial point is that the representation of the fermion field now contains a vertex operator:

$$\Psi(x) \sim d^\dagger(x) \sim \tilde{d}^\dagger(x) e^{-i\sqrt{2\pi\nu}\Theta(x)}, \quad (31)$$

where

$$\Theta(x) = \tilde{\varphi}(x) + \tilde{\varphi}(-x) \quad (32)$$

and

$$\nu = \gamma^2/(4\pi^2 K). \quad (33)$$

After the unitary transformation, we can calculate correlations for the free fields using standard methods. The Green's function for the free $\tilde{d}$ must be calculated with the proper mode expansion in terms of standing waves, $\tilde{d}(x) = \sqrt{(2/\pi)} \int_0^{k_0} dk \, \sin(kx)\tilde{d}_k$, where $k_0 \ll a^{-1}$ is the momentum cutoff of the impurity subband. We obtain

$$\langle \tilde{d}(x,t)\tilde{d}^\dagger(x,0)\rangle = e^{-i\epsilon t}\sqrt{\frac{-iM}{2\pi(t+i0)}}[1 - e^{i2Mx^2/(t+i0)}]. \quad (34)$$

In the bulk regime of Eq. (34), we neglect the rapidly oscillating factor $\propto e^{i2Mx^2/t}$; in this case, the free impurity propagator decays as $\sim t^{-1/2}$. In the boundary case, we expand for $x \sim a \ll \sqrt{t/M}$ and the free impurity propagator decays as $\sim t^{-3/2}$. This faster decay is due to the vanishing of the wave function at the boundary. It can also be understood by noting that at the boundary the impurity correlator can be calculated as

$$\langle \tilde{d}(a,t)\tilde{d}^\dagger(a,0)\rangle \sim a^2 \langle \partial_x\tilde{d}(0,t)\partial_x\tilde{d}^\dagger(0,0)\rangle, \quad (35)$$

and each spatial derivative amounts to an extra factor of $t^{-1/2}$ due to the quadratic dispersion of the band-edge mode.

In addition to the free impurity propagator, we have to consider the correlator [52,53,69]

$$\langle e^{\pm i\sqrt{2\pi\nu}\Theta(x,t)} e^{\mp i\sqrt{2\pi\nu}\Theta(x,0)}\rangle \propto \left|\frac{x^2}{t^2(4x^2 - v^2t^2)}\right|^\nu. \quad (36)$$

Thus, in the bulk case $(2x \gg vt)$, the correlator for the vertex operator adds a factor of $\sim t^{-2\nu}$ to the decay of the Green's functions. In the boundary case, the factor is $\sim t^{-4\nu}$, a faster decay that stems from the correlation between $\tilde{\varphi}(x)$ and $\tilde{\varphi}(-x)$ for $x \sim a$ (whereas these become uncorrelated right- and left-moving bosons in the bulk). Putting the effects together leads to

$$G_{\text{osc}}(t,a) \sim \langle \tilde{d}(a,\pm t)\tilde{d}^\dagger(a,0)\rangle \langle e^{i\sqrt{2\pi\nu}\Theta(a,t)} e^{-i\sqrt{2\pi\nu}\Theta(a,0)}\rangle$$

$$\sim e^{\mp i\epsilon t} t^{-\frac{3}{2}-4\nu}, \quad (37)$$

(where $\pm$ corresponds to particle/hole impurity), which is the result in Eqs. (13) and (15).

The scaling dimension of the vertex operator $e^{-i\sqrt{2\pi\nu}\Theta}$ can be related to a phase shift of the low-energy modes due to scattering with the d hole, establishing a connection with the orthogonality catastrophe [20]. For the integrable model in Eq. (7), the exact phase shift is a simple function of the Luttinger parameter [22]:

$$\gamma = \pi(1-K), \quad (38)$$

where the exact Luttinger parameter is for $0 \leqslant V \leqslant 1$

$$K = \frac{\pi}{2(\pi - \arccos V)}. \quad (39)$$

The renormalized band edge frequency is

$$\epsilon = \frac{\pi\sqrt{1-V^2}}{2\arccos V}. \quad (40)$$

The exact velocity of the low-energy modes and the effective mass of the impurity are also known: $v = M^{-1} = \epsilon$ (in units where $a = 1$).

In the free fermion limit, a particle tunneling into or out of the system is restricted to the free or occupied single-particle states. As is visible in Fig. 2 and Eq. (6) the LDOS is then identically zero outside of the bandwidth set by the dispersion relation. Turning on interactions allows for tunneling processes in which the particle leaving or entering the system excites additional particle-hole pairs. This leads to a small but nonzero value for the LDOS beyond the threshold energies. The effect can be included by carefully tracking the regulators in the Luttinger liquid correlator

$$\langle e^{i\sqrt{2\pi\nu}\varphi(x,t)} e^{-i\sqrt{2\pi\nu}\varphi(x,0)}\rangle \propto [i(vt-i0)]^{-\nu} \quad (41)$$

and the impurity correlator in Eq. (34). At the boundary and around the band minimum, the LDOS can for instance be expressed as

$$\rho(\omega \approx -\epsilon, a) \sim \int_{-\infty}^\infty dt \, \frac{e^{i(\omega+\epsilon)t}}{(vt+i0)^{4\nu}(t-i0)^{\frac{3}{2}}}$$

$$\sim [\theta(\omega+\epsilon) - \sin(4\pi\nu)\theta(-\omega-\epsilon)]|\omega+\epsilon|^{\frac{1}{2}+4\nu}. \quad (42)$$

We see that the shoulder ratio of the two-sided singularity is determined by an interplay of both the impurity and the low-energy propagators. This is similar, but slightly different than the two-sided singularities within the continuum of the spectral function and the dynamic structure factor [24] for which the shoulder ratio is determined by the exponents for right and left movers and the impurity propagator is just a delta function.

IV. OTHER CORRELATION FUNCTIONS

The mobile impurity model in Eq. (23) can be used to calculate the exponents in the long-time decay and finite-energy singularities of several dynamical correlation functions [46]. The general recipe for U(1)-symmetric models is to (i) identify the operator in the effective field theory that excites the band edge mode and carries the correct quantum numbers; (ii) write the operator in terms of free impurity and free bosons after the unitary transformation; (iii) compute the correlator using the folding trick in the boundary case. In this section, we apply this approach to calculate the exponents in the density autocorrelation of spinless fermions, spin autocorrelations of spin chains, and the single-particle Green's function of spinful fermions.

A. Density-density correlation

Let us now consider the density autocorrelation

$$C(t,x) \equiv \langle n(x,t)n(x,0) \rangle. \qquad (43)$$

Using the mode expansion in Eq. (17), we obtain the expression for the density operator including high-energy excitations

$$\begin{aligned} n(x) &= \Psi^\dagger(x)\Psi(x) \\ &\sim \psi_R^\dagger \psi_R + \psi_L^\dagger \psi_L + (e^{i2k_F x}\psi_L^\dagger \psi_R + \text{H.c.}) \\ &\quad + [(e^{-ik_F x}\psi_R^\dagger + e^{ik_F x}\psi_L^\dagger)d^\dagger + \text{H.c.}], \end{aligned} \qquad (44)$$

where $k_F = \pi/(2a)$ for the half-filled chain in the model of Eq. (7) and we omitted operators that annihilate the ground state (a vacuum of d particles). In the boundary case, ψ_L and ψ_R are identified according to Eq. (21). The leading operator generated by the low-energy part of $n(x)$ at the boundary is $\sim \partial_x \varphi(0)$, a dimension-one operator. As a result, the LL theory predicts the decay $\langle n(a,t)n(a,0) \rangle \sim 1/t^2$. By contrast, in the bulk case, the $2k_F$ part of $n(x)$ has dimension K and gives rise to $\langle n(x \gg a,t)n(x \gg a,0) \rangle \sim 1/t^{2K}$ as the leading contribution for repulsive interactions [5]. In summary, the low-energy term in the density autocorrelation is

$$C_{\text{LL}}(t,x) \sim t^{-\beta}, \qquad (45)$$

with exponents

$$\beta_{\text{end}} = 2, \quad \beta_{\text{bulk}} = 2K. \qquad (46)$$

On the other hand, the high-energy term in the mode expansion for the density at the boundary yields

$$\begin{aligned} n(a) &\sim d^\dagger(a)[e^{-ik_F a}\psi_R^\dagger(a) - e^{ik_F a}\psi_R^\dagger(-a)] + \text{H.c.} \\ &\sim \sin(k_F a)d^\dagger(a)\psi_R^\dagger(a) + \text{H.c..} \end{aligned} \qquad (47)$$

After bosonizing and performing the unitary transformation, we find that the high-energy term is given by

$$\begin{aligned} n(a) &\sim \tilde{d}^\dagger(a)\exp\left[i\sqrt{\frac{\pi}{2}}\left(\frac{1-\gamma/\pi}{\sqrt{K}} + \sqrt{K}\right)\varphi(a)\right] \\ &\quad \times \exp\left[i\sqrt{\frac{\pi}{2}}\left(\frac{1-\gamma/\pi}{\sqrt{K}} - \sqrt{K}\right)\varphi(-a)\right] + \text{H.c.} \\ &\sim a\partial_x\tilde{d}^\dagger(0)\exp\left[i\sqrt{2\pi}\left(\frac{1-\gamma/\pi}{\sqrt{K}}\right)\varphi(0)\right] + \text{H.c.}, \end{aligned} \qquad (48)$$

where we kept the leading operator in the expansion of the slowly-varying fields. From Eq. (48), it is straightforward to show that the autocorrelation function contains a term oscillating with the frequency of the high-energy hole:

$$C_{\text{osc}}(t,x) \sim e^{-i\epsilon t}t^{-\bar{\beta}}, \qquad (49)$$

with the boundary exponent

$$\bar{\beta}_{\text{end}} = \frac{3}{2} + \frac{(1-\gamma/\pi)^2}{K}. \qquad (50)$$

This should be compared with the corresponding exponent in the bulk case [22],

$$\bar{\beta}_{\text{bulk}} = \frac{1+K}{2} + \frac{(1-\gamma/\pi)^2}{2K}. \qquad (51)$$

Therefore the exponents associated with the frequency-ϵ oscillating term in the density autocorrelation obey the relation

$$2\bar{\beta}_{\text{bulk}} - \bar{\beta}_{\text{end}} = K - \tfrac{1}{2}. \qquad (52)$$

As mentioned in Sec. III, in lattice models we also have to consider the band-edge mode corresponding to a particle at the top of the band. In this case, the density operator contains an additional term that creates two high-energy modes, namely a hole at $k = 0$ and a particle at $k = \pi$. In the noninteracting bulk case of Hamiltonian (3), this term yields a contribution that behaves as $\sim e^{-i2\epsilon_0 t}/t$, where the slow $1/t$ decay stems from the propagators of the high-energy particle and hole. However, in the presence of a repulsive interaction $V > 0$, the decay of this contribution changes to $\sim e^{-i2\epsilon t}/t^2$ and decays faster than the frequency-ϵ term for $t \gg 1/(Ma^2 V^2)$ [22]. In the boundary case, the equivalent contribution is subdominant even in the noninteracting case, where it becomes $\sim e^{-i2\epsilon_0 t}/t^3$ due to the faster $t^{-3/2}$ decay of the free impurity propagator at the boundary. Therefore the long-time decay of the density autocorrelation $C(t,x = a)$ is well described by a combination of the LL term in Eq. (45) and the frequency-ϵ term in Eq. (49).

For the integrable model in Eq. (7), we can calculate the exponents $\bar{\beta}_{\text{bulk/end}}$ using Eqs. (38) and (39). We also note that the power-law decay of $C_{\text{osc}}(t,x)$ implies a finite-energy nonanalyticity in the Fourier transform

$$C(\omega,x) \sim |\omega - \epsilon|^{\bar{\beta}-1}. \qquad (53)$$

B. Spin autocorrelations

As an application of our theory to spin chains, we consider the spin-1/2 XXZ model with an open boundary

$$H_{\text{XXZ}} = \sum_{j \geq 1}\left[\frac{1}{2}(S_j^+ S_{j+1}^- + \text{H.c.}) + \Delta S_j^z S_{j+1}^z\right], \qquad (54)$$

where $\mathbf{S}_j$ is the spin operator on site j and Δ is the anisotropy parameter. We are interested in the long-time decay of the longitudinal ($\parallel$) and transverse ($\perp$) spin autocorrelations

$$C^{\parallel}(t,j) \equiv \langle S_j^z(t)S_j^z(0) \rangle, \qquad (55)$$

$$C^{\perp}(t,j) \equiv \langle S_j^+(t)S_j^-(0) \rangle. \qquad (56)$$

We focus on the critical regime $0 \leqslant \Delta \leqslant 1$. Via a Jordan-Wigner transformation [5]

$$S_j^z = \Psi^\dagger(j)\Psi(j) - \tfrac{1}{2}, \tag{57}$$

$$S_j^- = (-1)^j \Psi(j) e^{i\pi \sum_{l<j} \Psi^\dagger(l)\Psi(l)}, \tag{58}$$

the XXZ model is equivalent to the spinless fermion model in Eq. (7) with interaction strength $V = \Delta$. Thus, for $\Delta = 0$ (the XX chain), the model is equivalent to free fermions and some time-dependent correlations can be calculated exactly [80,81]. For $0 < \Delta \leqslant 1$, the LL approach predicts the asymptotic decay of nonoscillating terms in the spin autocorrelations [53]:

$$C_{\text{LL}}^{\parallel}(t,j) \sim t^{-\beta^{\parallel}}, \quad C_{\text{LL}}^{\perp}(t,j) \sim t^{-\beta^{\perp}}, \tag{59}$$

with exponents

$$\beta_{\text{end}}^{\parallel} = 2, \quad \beta_{\text{bulk}}^{\parallel} = 2K, \tag{60}$$

$$\beta_{\text{end}}^{\perp} = \frac{1}{K}, \quad \beta_{\text{bulk}}^{\perp} = \frac{1}{2K}, \tag{61}$$

where the exact Luttinger parameter is given by Eq. (39) with $V = \Delta$. Notice that the exponents for transverse and longitudinal autocorrelations coincide at the SU(2) point $\Delta = 1$, where $K = 1/2$.

The high-energy contributions to the spin operator can be obtained starting from Eqs. (57) and (58) and employing the mode expansion for the fermionic field in Eq. (17) [46]. In the bulk case, we find

$$S_{j=x}^z \sim \tilde{d}^\dagger(x) \exp\left[i\sqrt{\frac{\pi}{2}}\left(\frac{1+K-\gamma/\pi}{\sqrt{K}}\right)\varphi(x)\right]$$
$$\times \exp\left[i\sqrt{\frac{\pi}{2}}\left(\frac{1-K-\gamma/\pi}{\sqrt{K}}\right)\varphi(-x)\right] + \text{H.c.}, \tag{62}$$

$$S_{j=x}^- \sim \tilde{d}^\dagger(x) \exp\left[-i\sqrt{\frac{\pi}{2}}\left(\frac{K+\gamma/\pi}{\sqrt{K}}\right)\varphi(x)\right]$$
$$\times \exp\left[i\sqrt{\frac{\pi}{2}}\left(\frac{K-\gamma/\pi}{\sqrt{K}}\right)\varphi(-x)\right]. \tag{63}$$

At the boundary, we obtain

$$S_1^z \sim \partial_x \tilde{d}^\dagger(0) \exp\left[-i\sqrt{2\pi}\left(\frac{1-\gamma/\pi}{\sqrt{K}}\right)\varphi(0)\right] + \text{H.c.}, \tag{64}$$

$$S_1^- \sim \partial_x \tilde{d}^\dagger(0) \exp\left[-i\sqrt{2\pi}\left(\frac{\gamma}{\pi\sqrt{K}}\right)\varphi(0)\right]. \tag{65}$$

Calculating the correlators along the same lines as the previous examples, we obtain the oscillating terms in the autocorrelations

$$C_{\text{osc}}^{\parallel}(t,j) \sim e^{-i\epsilon t} t^{-\bar{\beta}^{\parallel}}, \tag{66}$$

$$C_{\text{osc}}^{\perp}(t,j) \sim e^{-i\epsilon t} t^{-\bar{\beta}^{\perp}}, \tag{67}$$

where

$$\bar{\beta}_{\text{end}}^{\parallel} = \frac{3}{2} + \frac{(1-\gamma/\pi)^2}{K}, \tag{68}$$

$$\bar{\beta}_{\text{end}}^{\perp} = \frac{3}{2} + \frac{(\gamma/\pi)^2}{K}. \tag{69}$$

We also present, for comparison, the previously known exponents in the bulk [22,82]:

$$\bar{\beta}_{\text{bulk}}^{\parallel} = \frac{1+K}{2} + \frac{(1-\gamma/\pi)^2}{2K}, \tag{70}$$

$$\bar{\beta}_{\text{bulk}}^{\perp} = \frac{1+K}{2} + \frac{(\gamma/\pi)^2}{2K}. \tag{71}$$

The results for the longitudinal spin autocorrelation are the same as those for the density autocorrelation derived in Sec. IV A, as expected from the mapping in Eq. (57). The bulk and boundary exponents for the spin autocorrelations obey a relation equivalent to Eq. (52)

$$2\bar{\beta}_{\text{bulk}}^{\perp/\parallel} - \bar{\beta}_{\text{end}}^{\perp/\parallel} = K - \frac{1}{2}, \tag{72}$$

which is independent of γ.

For the XXZ model, we can simplify the result for the exponents using the exact phase shift in Eq. (38). The bulk exponents become

$$\bar{\beta}_{\text{bulk}}^{\parallel} = K + \frac{1}{2}, \tag{73}$$

$$\bar{\beta}_{\text{bulk}}^{\perp} = K + \frac{1}{2K} - \frac{1}{2}. \tag{74}$$

Our new results for the boundary exponents are

$$\bar{\beta}_{\text{end}}^{\parallel} = K + \frac{3}{2}, \tag{75}$$

$$\bar{\beta}_{\text{end}}^{\perp} = K + \frac{1}{K} - \frac{1}{2}. \tag{76}$$

C. Green's function for spinful fermions

We now consider interacting spin-1/2 fermions, as described by the Hubbard model

$$H = -\sum_{x \geqslant 1} \sum_{\sigma=\uparrow,\downarrow} [\Psi_\sigma^\dagger(x)\Psi_\sigma(x+1) + \text{H.c.}]$$
$$+ U \sum_{x \geqslant 1} n_\uparrow(x) n_\downarrow(x), \tag{77}$$

where $U > 0$ is the repulsive on-site interaction. Away from half-filling and in the absence of an external magnetic field, the low-energy spectrum is described by two bosonic fields corresponding to decoupled charge and spin collective modes. Our purpose here is to illustrate the effects of spin-charge separation on finite-energy contributions to time-dependent correlation functions. We focus on the single-particle Green's function

$$G_\uparrow(t,x) = \langle\{\Psi_\uparrow(x,t), \Psi_\uparrow^\dagger(x,0)\}\rangle. \tag{78}$$

In the case of spinful fermions, singular features of dynamic correlations can in principle come from both spinon and holon

impurities interacting with the low-energy modes [27,28,83]. For repulsive interactions, the spin velocity is smaller than the charge velocity [5], so the lower threshold of the spinon-holon continuum is expected to correspond to a finite-energy spinon impurity rather than a holon. Here we focus on the contribution from a single high-energy spinon to the Green's function and to the LDOS. It is implicitly assumed that the fermion-fermion interactions are strong enough that there is a sizable separation between the spinon band edge and the holon band edge. Otherwise, weak interactions would imply a small energy scale for spin-charge separation, making it difficult to resolve the two contributions in real time or in the frequency domain.

We follow the construction in Ref. [83] to define the operators that create finite-energy spinons coupled to low-energy charge and spin bosons, maintaining the correct quantum numbers. Starting from bosonization expressions like

$$\psi_{R,\sigma} \sim e^{-i\sqrt{2\pi}\phi_{R\sigma}}, \tag{79}$$

we go to a spin and charge separated basis. The physical field is expanded in right and left movers and written in terms of charge and spin degrees of freedom. We will only need the right moving component for which the spinon part is projected onto the impurity operator. This leads to the projection

$$\Psi_\uparrow \sim d_s^\dagger e^{-i\sqrt{\pi}(\frac{1}{2}\Phi_s^* - \frac{1}{2}\Phi_c^* + \Theta_c^*)}. \tag{80}$$

Here, Φ_ν^* and Θ_ν^*, with $\nu = c,s$ for charge or spin, respectively, are the conjugate bosonic fields that diagonalize the Hamiltonian at the Luther-Emery point where spin and charge modes are exactly separated. The bosonic fields satisfy $[\partial_x \Phi_\nu^*(x), \Theta_{\nu'}^*(x')] = i\delta_{\nu\nu'}\delta(x - x')$.

The impurity model is

$$
\begin{aligned}
H_{\text{MIM}} = &\int_0^\infty dx \sum_{\nu=c,s} \frac{v_\nu}{2}\left[\frac{1}{2K_\nu}(\partial_x \Phi_\nu^*)^2 + 2K_\nu(\partial_x \Theta_\nu^*)^2\right] \\
&+ \int_0^\infty dx\, d_s^\dagger\left(\epsilon_s + \frac{\partial_x^2}{2M_s}\right)d_s \\
&+ \int_0^\infty dx \sum_\nu \frac{v f_\nu}{\sqrt{\pi}} d_s^\dagger d_s \partial_x \Phi_\nu^*,
\end{aligned}
\tag{81}
$$

where $v_{c,s}$ are the charge and spin velocities, respectively, $K_{c,s}$ are the Luttinger parameters, ϵ_s and $-M_s$ are the energy and effective mass of the high-energy spinon, and $f_{c,s}$ are impurity-boson coupling constants. At the Luther-Emery point with free holons and spinons [83], we have $K_c = K_s = 1/2$ and $f_c = f_s = 0$. In contrast, SU(2)-symmetric models correspond to strongly interacting spinons.

We decouple the impurity mode by the unitary transformation

$$U = \exp\left(-i\sum_\nu \frac{K_\nu f_\nu}{v_\nu \sqrt{\pi}}\int_0^\infty dx\, d_s^\dagger d_s \Theta_\nu^*\right). \tag{82}$$

We then implement the boundary conditions by the folding trick and diagonalize the low-energy part of the Hamiltonian by a canonical transformation. We define

$$\gamma_\nu = \frac{K_\nu f_\nu}{v_\nu}. \tag{83}$$

The final expression for the projection of the spinful fermion field operator is

$$
\begin{aligned}
\Psi_\uparrow(x) \sim \tilde{d}_s^\dagger(x)\exp&\left[\left(-\frac{\sqrt{2K_s}}{4} + \frac{\gamma_s}{\pi\sqrt{2K_s}}\right)\varphi_s(x)\right. \\
&+ \left(\frac{\sqrt{2K_s}}{4} + \frac{\gamma_s}{\pi\sqrt{2K_s}}\right)\varphi_s(-x) \\
&+ \left(\frac{1}{2\sqrt{2K_c}} + \frac{\sqrt{2K_c}}{4} + \frac{\gamma_c}{\pi\sqrt{2K_c}}\right)\varphi_c(x) \\
&+ \left.\left(\frac{1}{2\sqrt{2K_c}} - \frac{\sqrt{2K_c}}{4} + \frac{\gamma_c}{\pi\sqrt{2K_c}}\right)\varphi_c(-x)\right]. \quad (84)
\end{aligned}
$$

Here, $\varphi_{c,s}(x)$ represent the free low-energy charge and spin modes after decoupling of the impurity and $\tilde{d}_s^\dagger$ creates the decoupled spinon mode.

The exponents for the corresponding oscillating contribution of $G_\uparrow(t,x)$ are easily read off from Eq. (84). Let us restrict ourselves to the SU(2) invariant case appropriate for the Hubbard model at zero magnetic field. In this case, $K_s = 1$ and $\gamma_s = -\pi/2$. We obtain

$$G(t,x) \sim e^{-i\epsilon_s t} t^{-\nu^{(s)}}, \tag{85}$$

with

$$\nu_{\text{bulk}}^{(s)} = 1 + \frac{K_c}{4} + \frac{1}{4K_c}\left(1 + \frac{2\gamma_c}{\pi}\right)^2, \tag{86}$$

$$\nu_{\text{end}}^{(s)} = 2 + \frac{1}{2K_c}\left(1 + \frac{2\gamma_c}{\pi}\right)^2. \tag{87}$$

The singular behavior of the LDOS is obtained by Fourier transformation as before. We also obtain the relation

$$2\nu_{\text{bulk}}^{(s)} - \nu_{\text{end}}^{(s)} = \frac{K_c}{2}, \tag{88}$$

which is independent of γ_c. It would be interesting to test this prediction numerically and investigate the relative importance of the spinon and holon impurity configuration for the autocorrelation and LDOS of the Hubbard model.

V. ROLE OF INTEGRABILITY

Our results predict the exponents of autocorrelation functions at the boundary of critical one-dimensional systems *assuming* that the long-time decay is described by a power law. By Fourier transform, the same theory predicts the exponent of the nonanalyticity at the finite energy $\omega = \epsilon$ in the frequency domain. We expect this to hold for integrable models, where one can calculate a well-defined band-edge frequency from the renormalized dispersion relation (or dressed energy) for the elementary excitations. Examples of integrable models with open boundary conditions include the open XXZ chain [84,85] in Eq. (54) [or, equivalently, its fermionic version in Eq. (7)] and the Hubbard model [86] in Eq. (77), on which many of the previous studies of local spectral properties are based.

In generic, nonintegrable models, the persistence of a nonanalyticity inside a multiparticle continuum is questionable. It has been argued that a finite-energy singularity can be protected in 1D systems by conservation of quantum numbers in high-energy bands [87]. However, the high-energy
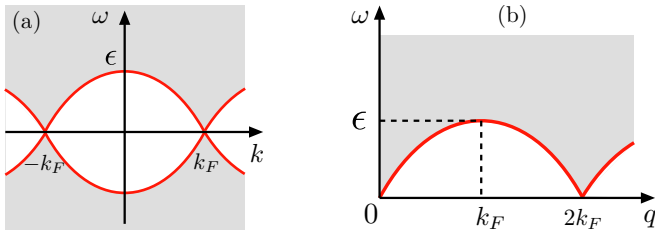
FIG. 3. (a) Support of the single-fermion spectral function $A(k,\omega)$ for a generic 1D model of interacting fermions with Fermi momentum k_F. The solid red line represents the lower threshold $\omega_-(k)$, below which $A(k,\omega)$ vanishes. The band edge frequency can be identified as $\epsilon = \omega_-(k=0)$. (b) Support of the dynamical structure factor $S(q,\omega)$.

subband in our effective mobile impurity model is defined by a projection of the band edge modes, which carry the same quantum numbers as the low-energy modes. Thus, strictly speaking, there is no conservation law associated with the number of d particles.

Nonetheless, we can argue that the band edge is still well defined for bulk correlations in a semi-infinite system. In the bulk, one can measure momentum-resolved response functions, for instance the spectral function

$$A(k,\omega) = \frac{1}{2\pi} \int_{-\infty}^{\infty} dt\, e^{i\omega t} \sum_y e^{-iky}$$
$$\times \langle \{\Psi(x+y,t), \Psi^\dagger(x,0)\} \rangle, \quad (89)$$

or the dynamical structure factor

$$S(q,\omega) = \frac{1}{2\pi} \int_{-\infty}^{\infty} dt \sum_y e^{-iqy} \langle n(x+y,t)n(x) \rangle. \quad (90)$$

In momentum-resolved dynamical correlations, the spectral weight vanishes identically below a lower threshold [46] [see Fig. 3(a)]. This threshold is defined by kinematic constraints and exists even for nonintegrable models. The mobile impurity model in the bulk then predicts a power-law singularity as the frequency approaches the threshold from above. For instance, for the positive-frequency part of the spectral function [24]:

$$A(k,\omega) \sim [\omega - \omega_-(k)]^{-1+2\nu}, \quad (91)$$

with ν defined in Eq. (33). The band edge frequency that governs the oscillations in local correlations can be identified from the spectrum as a local maximum in the lower threshold, about which the threshold is approximately parabolic. For the spectral function, this happens for $k \approx 0$:

$$\omega_-(k \approx 0) \approx \epsilon - \frac{k^2}{2M}. \quad (92)$$

In the dynamical structure factor, the band edge can be read off from the value of the lower threshold at momentum $q = k_F$, corresponding to the excitation composed of a hole at $k = 0$ and a particle at the Fermi point $k = k_F$ [Fig. 3(b)].

The nonanalyticities in the local bulk correlations are related to the threshold singularities of the momentum-resolved correlations by integration over momentum. For instance, integrating the spectral function implies that the

LDOS behaves as

$$\rho(\omega, x \gg a) = \int_{-\pi/a}^{\pi/a} dk\, A(k,\omega)$$
$$\sim \int_{-k_0}^{k_0} dk\, \theta\left(\omega - \epsilon + \frac{k^2}{2M}\right) \left|\omega - \epsilon + \frac{k^2}{2M}\right|^{-1+2\nu}$$
$$\sim |\omega - \epsilon|^{-\frac{1}{2}+2\nu}. \quad (93)$$

Since the singularities in the momentum-resolved dynamic response cannot be broadened, the power-law decay of autocorrelations in the bulk is a generic property of critical 1D systems.

However, since momentum is not conserved in the presence of a boundary, the above argument cannot be used to establish power-law decay of autocorrelation functions at the boundary. From the field theory perspective, the difference between bulk and boundary cases can be understood by analyzing the effects of boundary operators that perturb the mobile impurity model in Eq. (23). In the following, we shall argue that, although formally irrelevant, boundary operators introduce two important effects in nonintegrable models: (i) they may renormalize the frequency of oscillations in the boundary autocorrelation, which will then differ from the frequency in the bulk (only the latter being equal to the band edge frequency ϵ); (ii) boundary operators that do not conserve the number of particles in high-energy subbands may give rise to a decay rate for the mobile impurity, which implies exponential decay of the boundary autocorrelation in time and the associated broadening of the nonanalyticity in the frequency domain.

For discussion purposes, we will focus on the regime of weak interactions, which can be analyzed by perturbation theory in the free fermion basis, but the argument can be made more general by bosonizing the low-energy sector and the main points carry through. If we are interested in the impurity decay, we can furthermore safely neglect operators that involve the impurity field but do not couple it to the low-energy modes— these will at most renormalize the impurity dispersion.

As a simple example of a boundary operator respecting the symmetries and boundary conditions, consider the impurity-number-conserving perturbation

$$\partial H = g\, \partial_x d^\dagger(0) \partial_x d(0) \psi^\dagger(0) \psi(0). \quad (94)$$

Here we use $\psi(x) = \psi_R(x) = -\psi_L(-x)$ to denote the low-energy modes of the fermion field on the unfolded line. We will assume that ∂H is present in the effective Hamiltonian and analyze its influence on the impurity propagator in perturbation theory.

It is convenient to Fourier transform the time coordinate to make use of energy conservation, but not the space coordinate. We can organize the diagrammatic expansion of the time-ordered impurity propagator

$$G_d(x,x';t) = \langle T d(x,t) d^\dagger(x',0) \rangle \quad (95)$$

using the Dyson equation

$$G_d(x,x;\omega) = G_d^{(0)}(x,x;\omega) + \int dx_1 \int dx_2\, G_d^{(0)}(x,x_2;\omega)$$
$$\times \Sigma(x_2,x_1;\omega) G_d(x_1,x;\omega). \quad (96)$$

If we take only boundary operators into account, the self-energy Σ is purely local:

$$\Sigma(x_2,x_1;\omega) = \Sigma(\omega)\delta(x_1 - a)\delta(x_2 - a). \quad (97)$$

The solution of the Dyson equation for $x_1 = x_2 = a$ is

$$G_d(a,a;\omega) = \frac{1}{\left[G_d^{(0)}(a,a;\omega)\right]^{-1} - \Sigma(\omega)}. \quad (98)$$

It follows from Eq. (98) that the nonanalyticity in the LDOS will be broadened if the local self-energy $\Sigma(a,a;\omega)$ has a nonzero imaginary part at $\omega = \epsilon$.

For the continuation of this calculation, let us use the notation $G(t) = G(a,a;t)$ for boundary propagators. The free propagator for the d particle at the boundary is

$$G_d^{(0)}(t) = \frac{(-iM)^{3/2}}{\sqrt{2\pi}}\frac{\theta(t)e^{-i\epsilon t}}{(t + i\eta/v)^{3/2}}, \quad (99)$$

while for the low-energy modes, we have

$$G_{LL}^{(0)}(t) \equiv \langle T\psi(a,t)\psi^\dagger(a,0)\rangle = [2\pi i(vt - i\eta \, \mathrm{sgn}\, t)]^{-1}, \quad (100)$$

where η is a short-distance cutoff and is related to the bandwidth of the impurity and low-energy subbands.

The first-order correction in the coupling constant g corresponds to a tadpole diagram proportional to the density of low-energy modes at the boundary. It will not induce the decay rate that we are after [rather, it is like a nonuniversal renormalization of the coupling constant of the boundary operator $\partial_x d^\dagger(0)\partial_x d(0)$, which does not couple the impurity to the low-energy modes]. The second-order correction is given by the expression

$$\delta\Sigma^{(2)}(\omega) = -ig^2\int_{-\infty}^{\infty}dt\, e^{i\omega t}G_{LL}^{(0)}(t)G_{LL}^{(0)}(-t)G_d^{(0)}(t). \quad (101)$$

The imaginary part is then obtained as

$$\mathrm{Im}\,\delta\Sigma^{(2)} = -\left(\frac{g}{2\pi}\right)^2\frac{M^{3/2}}{\sqrt{\pi}}$$
$$\times\int_{-\infty}^{\infty}dt\frac{e^{i(\omega-\epsilon)t}}{(vt - i\eta)(vt + i\eta)(t + i\eta/v)^{3/2}}. \quad (102)$$

By power counting in the integral we see that

$$\delta\Sigma^{(2)}(\omega) \propto |\epsilon - \omega|^{5/2}, \quad (103)$$

and hence the self-energy vanishes on-shell, when $\omega = \epsilon$, so this correction will not induce a finite decay rate

$$\frac{1}{\tau} = -\,\mathrm{Im}\,\Sigma(\omega = \epsilon). \quad (104)$$

The factor of $e^{i(\omega-\epsilon)t}$ in Eq. (102) is general for self-energy contributions generated by perturbations that conserve the number of d particles. Therefore the decay rate must vanish to all orders if, for some reason, the irrelevant interactions conserve the number of high-energy excitations [87].

To derive a nonzero decay rate, we will have to consider perturbations that do not preserve the number of impurity modes and may contribute to the self-energy for $\omega = \epsilon$. As stated before, this is a typical effect of the boundary breaking

translational invariance, since in the bulk kinematic constraints associated with momentum and energy conservation prevent the decay of the band-edge mode. Due to the U(1) symmetry (conservation of the total charge), the annihilation (creation) of a high-energy hole entails the annihilation (creation) of a particle in a low-energy state. A family of such boundary operators that are allowed by symmetry and the boundary conditions are, for example,

$$\partial H_n = g_n\partial_x d(0)[\psi^\dagger(0)\psi(0)]^n\psi(0) + \mathrm{H.c.} \quad (105)$$

The first nontrivial correction to the self-energy is of second order in the coupling g_n. The diagram corresponds to a simple low-energy propagator dressed by n particle-hole pairs,

$$\delta\Sigma_n^{(2)}(\omega) = -ig_n^2\int_{-\infty}^{\infty}dt\, e^{i\omega t}\left[G_{LL}^{(0)}(t)\right]^{n+1}\left[G_{LL}^{(0)}(-t)\right]^n, \quad (106)$$

leading to

$$\mathrm{Im}\,\delta\Sigma_n^{(2)}(\omega) = -\frac{g_n^2}{(2\pi v)^{2n+1}}\int_{-\infty}^{\infty}dt\frac{te^{i\omega t}}{i(t^2 + \eta^2/v^2)^{n+1}}. \quad (107)$$

Closing the contour in the upper half plane and picking up the pole at $t = i\eta/v$, we obtain a cutoff-dependent decay rate

$$\frac{1}{\tau} \propto g_n^2 e^{-\epsilon\eta/v}. \quad (108)$$

In contrast to the earlier case, we do find a possibly finite decay rate. We note that $\epsilon\eta/v \sim \mathcal{O}(1)$ if the short-distance is of the order of the lattice spacing a, but $\epsilon\eta/v \gg 1$ if $\eta \gg a$.

Boundary operators like ∂H_n will in principle be generated from lower-order processes for a generic model when we integrate out the states outside of our impurity and low-energy subbands in a renormalization group procedure. Physically, we can think of these processes as the result of a cascade, or particle shower [88,89], involving many intermediate states, which are no longer in the description. The number n of low-energy particle-hole pairs roughly reflects the number of microscopic interaction processes and has to be sizable (of the order of $\sim v\eta^{-1}\epsilon^{-1}$) to accommodate for the excess energy. The coupling g_n, therefore, will scale with high powers of the microscopic interaction strength and thus will be very small for weak interactions leading to a negligible decay rate. Stronger interactions, however, may show sizable renormalization effects in the decay rate and frequency shift of correlations at the boundary.

Coming back to integrability, we argue that the above corrections do not occur for models with open boundary conditions solvable by Bethe ansatz. The argument relies on the fact that the exact eigenstates of the model still define a conserved impurity state corresponding to a hole in the quantum number configuration of the ground state. This state is parametrized by a rapidity λ and has well-defined energy given by the dressed energy function $\epsilon(\lambda)$. One can in fact show, using the thermodynamic Bethe ansatz, that the spectrum is still determined by the bulk dressed energy function by a similar type of folding trick to the one we used for the low-energy theory [90]. Not only does this imply the absence of a decay rate, also the impurity energy does not renormalize and the same frequency should be observed in the autocorrelation in the bulk and at the boundary. The "miracle" of integrability

thus manifests itself as a fine tuning of the coupling constants in the effective field theory, in this case the vanishing of the couplings g_n.

VI. NUMERICAL RESULTS FOR SPIN CHAINS

In this section, the field theoretical prediction for the asymptotic behavior of the autocorrelations $C^{\parallel/\perp}(t,j)$ are checked, numerically, for critical spin chains with size $L = 300$ and open boundary conditions. We use the adaptive tDMRG [74,91] keeping up to $m = 300$ ($m = 450$) states per block for the chains with spin $S = 1/2$ ($S = 1$ and $3/2$). The time evolution was performed with the second-order Suzuki-Trotter decomposition with time step $0.025 \leqslant \delta t \leqslant 0.3$. The discarded weight was typically about 10^{-8}–10^{-12} during the time evolution. The numerical error sources in the tDMRG have two origins:

(1) The Trotter error, which is related with the order (n) of the Suzuki-Trotter decomposition. For the order n, this error is of the order $(\delta t)^{n+1}$.

(2) The truncation error associated with the number of discard states.

These errors can be controlled by decreasing the time step (δt) and increasing the number of states kept in the DMRG simulation.

We are interested in the long-time behavior of the longitudinal and transverse spin autocorrelations at the end site, $C_{\text{end}}^{\parallel/\perp}(t) = C^{\parallel/\perp}(t,1)$, and in the bulk, $C_{\text{bulk}}^{\parallel/\perp}(t) = C^{\parallel/\perp}(t,L/2)$. As discussed in the Sec. IV B, these autocorrelations can be described by a combination of universal power laws predicted by the LL theory and oscillating terms predicted by the nLL theory.

A. Integrable spin-1/2 model

First, we consider the integrable spin-1/2 XXZ model in Eq. (54). According to Eqs. (59), (66), and (67), the real parts of the autocorrelations behave as

$$\text{Re}[C_{\text{end}}^{\parallel}(t)] = \frac{A_1^{\parallel}}{t^2} + \frac{A_2^{\parallel}\cos(Wt+\varphi)}{t^{\frac{3}{2}+\xi}}, \tag{109}$$

$$\text{Re}[C_{\text{bulk}}^{\parallel}(t)] = \frac{B_1^{\parallel}}{t^2} + \frac{B_2^{\parallel}}{t^{2\xi}} + \frac{B_3^{\parallel}\cos(Wt+\varphi)}{t^{\frac{1}{2}+\xi}}$$
$$+ \frac{B_4^{\parallel}\cos(2Wt+\tilde{\varphi})}{t^{\zeta}}, \tag{110}$$

$$\text{Re}[C_{\text{end}}^{\perp}(t)] = \frac{A_1^{\perp}}{t^{\frac{1}{\xi}}} + \frac{A_2^{\perp}\cos(Wt+\varphi)}{t^{\xi+\frac{1}{\xi}-\frac{1}{2}}}, \tag{111}$$

$$\text{Re}[C_{\text{bulk}}^{\perp}(t)] = \frac{B_1^{\perp}}{t^{\frac{1}{2\xi}}} + \frac{B_2^{\perp}}{t^2} + \frac{B_3^{\perp}\cos(Wt+\varphi)}{t^{\xi+\frac{1}{2\xi}-\frac{1}{2}}}. \tag{112}$$

Here we have imposed the constraint that for the XXZ model the interaction dependence of all exponents (bulk or boundary, low-energy or high-energy) can be expressed in terms of a single parameter ξ. The theoretical prediction is $\xi = K = \frac{\pi}{2(\pi-\arccos\Delta)}$. The frequency of the oscillating terms is predicted to be the same for bulk and boundary autocorrelations, and is given by $W = \epsilon = \frac{\pi\sqrt{1-\Delta^2}}{2\arccos\Delta}$. In Eq. (110), we included the oscillating term with frequency $2W$, which comes from a
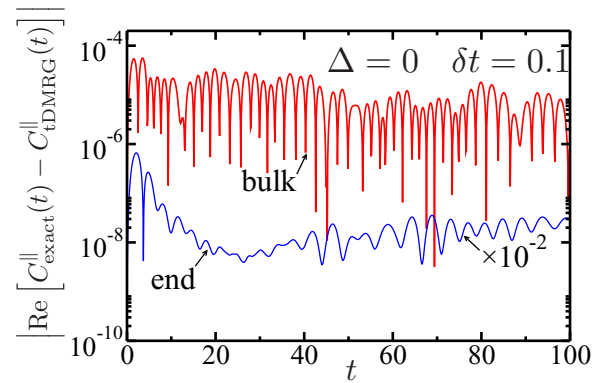

FIG. 4. The differences between the real parts of the exact results [Eq. (113)] and the tDMRG data for the autocorrelations $C^{\parallel}(t,j)$ for the spin-1/2 XXZ chain with $L = 300$ and $\Delta = 0$. The bulk (end) case corresponds to $j = L/2$ ($j = 1$). We use $m = 200$ DMRG states and time step $\delta t = 0.1$. We multiply the results of $C_{\text{end}}^{\parallel}(t)$ by 10^{-2} in order to see both data in the same figure.

hole at $k = 0$ and a particle at $k = \pi$ [22]. The corresponding exponent is predicted to be $\zeta = 1$ for $\Delta = 0$ but $\zeta = 2$ for $0 < \Delta < 1$ and $t \gg 1/\Delta^2$. In the following, we shall test the analytical predictions from the nLL theory by fitting the tDMRG data to the expressions above.

Before presenting the fit results, let us consider the chain with $\Delta = 0$. At this point, the autocorrelation $C^{\parallel}(t,j)$ is equivalent to the density autocorrelation for free spinless fermion (see Sec. II). It is straightforward to show that for even size L

$$C^{\parallel}(t,j) = \left[\frac{2}{L+1}\sum_{m=1}^{L/2}\sin^2\left(\frac{m\pi j}{L+1}\right)e^{i\varepsilon_m t}\right]^2, \tag{113}$$

where $\varepsilon_m = -\cos\left(\frac{\pi m}{L+1}\right)$. In Fig. 4, we present the differences between the exact results of $C_{\text{end/bulk}}^{\parallel}(t)$ and the tDMRG data obtained considering $m = 200$ and $\delta t = 0.1$. As we can see, the agreement is quite good. It is interesting to note that the errors are of the order $\sim 10^{-4}$–10^{-6}, which are smaller than the errors due to the use of the second-order Suzuki-Trotter decomposition, of order $(\delta t)^3 = 10^{-3}$.

The results depicted in Fig. 4 show that we obtain accurate results for the $C_{\text{end/bulk}}^{\parallel}(t)$ with the tDMRG by using $m = 200$ and $\delta t = 0.1$. Away from the point $\Delta = 0$, we do not have exact results to compare with. In this case, we compare the autocorrelations $C_{\text{end/bulk}}^{\parallel/\perp}(t)$ for different values of m ($m = 100$, 200, and 300) and time step δt ($\delta t = 0.3$, 0.1, and 0.025), in order to estimate the numerical errors. Overall, we estimate that these errors are at least one order of magnitude smaller than the values of the autocorrelations acquired by tDMRG.

Some typical examples of the numerical data fitted to Eqs. (109)–(112) are presented in Fig. 5 for the spin-1/2 XXZ chain with anisotropy $\Delta = 0.6$. The parameters ξ and W obtained by this fitting procedure are given in Table I for some values of the anisotropy Δ. Overall, the parameters obtained are in agreement with the theoretical prediction presented in the last column of Table I. In the fitting procedure, the tDMRG data considered were in the range $15 < t < 80$. We note that the parameter ξ changes slightly depending on the
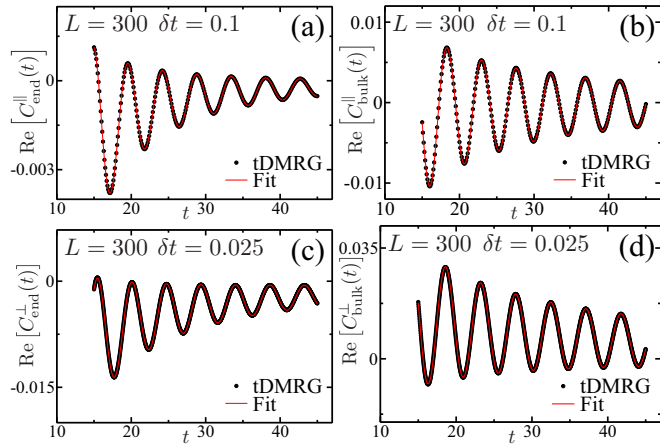
FIG. 5. Real parts of the autocorrelations $C_{\text{end/bulk}}^{\parallel/\perp}(t)$ vs t for the spin-1/2 XXZ chain for $\Delta = 0.6$, $L = 300$, and $m = 200$. For the longitudinal [(a) and (b)] and transverse [(c) and (d)] spin autocorrelations we use $\delta t = 0.1$ and 0.025, respectively. The symbols are the tDMRG results and the solid lines are fits to our data using Eqs. (109)–(112) (see text).
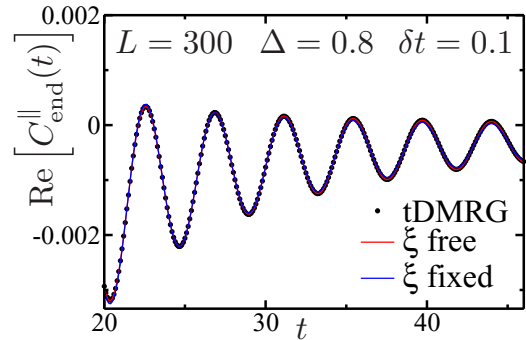

FIG. 6. Real part of the longitudinal spin autocorrelation $C_{\text{end}}^{\parallel}(t)$ vs t for the spin-1/2 XXZ chain with anisotropy $\Delta = 0.8$ and system size $L = 300$. The data were obtained using $m = 200$ DMRG states and time step $\delta t = 0.1$. We fit the tDMRG data to Eq. (109) taking the parameter ξ to be either free or fixed as $\xi = K$ (see legend).

time range used in the fit. One of the largest discrepancies found corresponds to the parameter ξ obtained from $C_{\text{end}}^{\parallel}(t)$ for $\Delta = 0.8$ (see Table I). Although this exponent ($\xi = 0.459$) differs slightly from the predicted ($K = 0.6287$), we found a very good agreement of the fit of the tDMRG data to Eq. (109) if we consider $\xi = K$ fixed, as shown in Fig. 6. It is also interesting to note that, even though for some values of Δ the fitted value of ξ is not so close to the predicted one, we found that $|2\beta_{\text{bulk}}^{\parallel/\perp} - \beta_{\text{end}}^{\parallel/\perp} - K + 1/2| < 0.06$, which is close to zero in agreement with the relation predicted in Eq. (72).

B. Effects of bound states and nearly flat bands

Before we start analyzing nonintegrable models, let us briefly describe some situations where the predictions of Sec. IV B do not hold. As mentioned in Sec. III, our mobile impurity model assumes that a single type of high-energy excitation (the deep hole) is sufficient to describe the oscillations in the autocorrelation functions. This is

TABLE I. The exponent ξ and the band edge frequency W for the autocorrelations $C_{\text{end/bulk}}^{\parallel/\perp}(t)$ for the spin-1/2 XXZ chain for some values of Δ. The parameters ξ and W were obtained by fitting the tDMRG data to Eqs. (109)–(112). The last column are the theoretical predictions for these parameters.

		$C_{\text{end}}^{\parallel}$	$C_{\text{bulk}}^{\parallel}$	$C_{\text{end}}^{\perp}$	$C_{\text{bulk}}^{\perp}$	Exact
$\Delta = 0$	ξ	0.992	1.006	0.943	0.981	1
	W	1.002	1.000	1.000	1.002	1
$\Delta = 0.3$	ξ	0.849	0.829	0.836	0.893	0.8375
	W	1.182	1.183	1.184	1.186	1.1835
$\Delta = 0.6$	ξ	0.677	0.678	0.711	0.595	0.7093
	W	1.355	1.355	1.356	1.358	1.3551
$\Delta = 0.8$	ξ	0.459	0.554	0.649	0.585	0.6287
	W	1.466	1.465	1.467	1.468	1.4646

equivalent to assuming that in the frequency domain, the dominant finite-energy nonanalyticity occurs at the band edge of single-hole excitations. However, more generally dynamical correlation functions may contain additional singularities at frequencies corresponding to bound states which are absent in the noninteracting model. In this case, additional oscillating components in the long-time decay of $C_{\text{end/bulk}}^{\parallel/\perp}(t)$ can arise and decay more slowly than the contribution considered in Eqs. (109)–(112). While bound states can be incorporated in a more general mobile impurity model [24], in this work we look for examples where the existence of bound states can be ruled out, so we can test the bulk versus boundary behavior of the band edge contribution.

The signature of bound states can be observed in the longitudinal spin structure factor

$$S^{\parallel}(q,\omega) = \frac{1}{2\pi} \int_{-\infty}^{\infty} dt \, e^{i\omega t} \sum_j e^{-iqj} C^{\parallel}(t,j). \quad (114)$$

It is known [22] that for the spin-1/2 XXZ chain with $-1 < \Delta < 0$, which is in the critical regime but is equivalent to spinless fermions with *attractive* interactions, $S^{\parallel}(q,\omega)$ exhibits a narrow peak above the two-spinon continuum. This peak can be interpreted within the effective field theory as a bound state of a high-energy particle and a high-energy hole. Figure 7 shows $S^{\parallel}(q,\omega)$ for $\Delta = -0.25$. Although this bound state is inside a continuum of multiple particle-hole pairs, we expect that for the integrable model the peak in the longitudinal spin structure factor is not broadened by decay processes and is given by a delta function, i.e., $S^{\parallel}(q,\omega) \sim \delta(\omega - \Omega_{\text{bs}}(q))$, where $\Omega_{\text{bs}}(q)$ is the dispersion relation of the bound state. In our numerical results we observe that the peak has a finite width because the frequency resolution is limited by the finite time in the tDMRG data. However, as shown in Fig. 7(b), $S^{\parallel}(q,\omega)$ becomes narrower as the time increases. This is a strong evidence of the existence of a bound state in the spectrum.

Another situation that limits the applicability of our mobile impurity model is when the excitation spectrum contains particles with a large effective mass M, i.e., in the presence of nearly flat bands. As discussed in Sec. III, the exponents of the oscillating terms hold for large times compared to the inverse
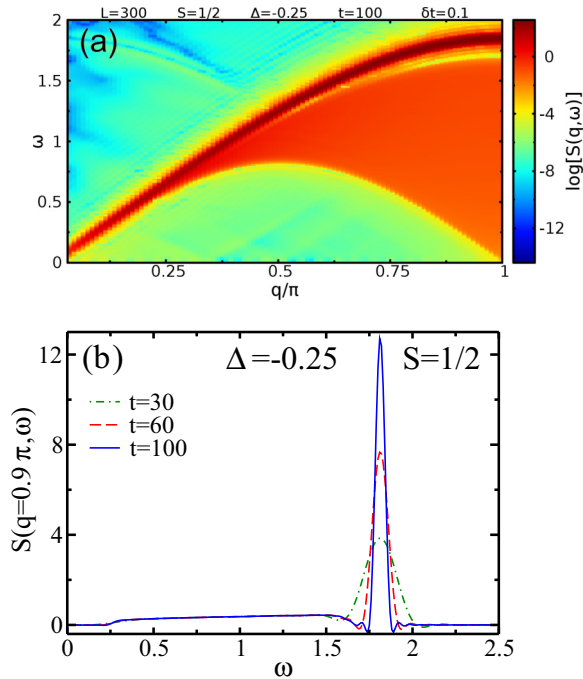
FIG. 7. (a) Longitudinal spin structure factor for the spin-1/2 XXZ chain with anisotropy $\Delta = -0.25$ and system size $L = 300$. The data were obtained using $m = 200$ and $\delta t = 0.1$. (b) Line shapes of $S(q = 0.9\pi, \omega)$ obtained for different maximum times.

of the band curvature energy scale, in the regime $t \gg Ma^2$. If the mass is large, the asymptotic behavior will only be observed after extremely long times, beyond the reach of the tDMRG method.

C. Higher-S spin chains

With the above limitations in mind, we turn to the study of autocorrelations in nonintegrable models. In principle, a simple way to break the integrability of the spin-1/2 XXZ chain (while preserving a gapless spectrum as well as U(1) and discrete symmetries) is to add small next-nearest-neighbor exchange couplings, e.g., $\delta H \sim \sum_j S_j^z S_{j+2}^z$. However, it is well known that the adaptive tDMRG only works efficiently for models with nearest-neighbor exchange couplings [92]. For this reason, we study critical spin-S chains with $S > 1/2$ [93–96] as examples of nonintegrable models. We consider the Hamiltonian

$$H = \sum_{j=1}^{L} \left[S_j^x S_{j+1}^x + S_j^y S_{j+1}^y + \Delta S_j^z S_{j+1}^z + D\left(S_j^z\right)^2 \right], \quad (115)$$

where $\mathbf{S}_j$ is the spin-S operators acting on site j, Δ is the exchange anisotropy and D is the single-ion anisotropy.

The expressions for spin-S operators within the low-energy effective field theory can be obtained by noting that spin chains with $S = n/2$ can be represented by n-leg ladders in the limit where strong rung couplings select the spin-S multiplet of the local spins 1/2 [95,97]. For instance, for $S = 1$ we can write $\mathbf{S}_j = \boldsymbol{\sigma}_j + \boldsymbol{\tau}_j$, where $\boldsymbol{\sigma}_j$ and $\boldsymbol{\tau}_j$ are two spin-1/2 operators that commute with each other, and use the Jordan-Wigner transformation [essentially two copies of Eqs. (57) and (58)]
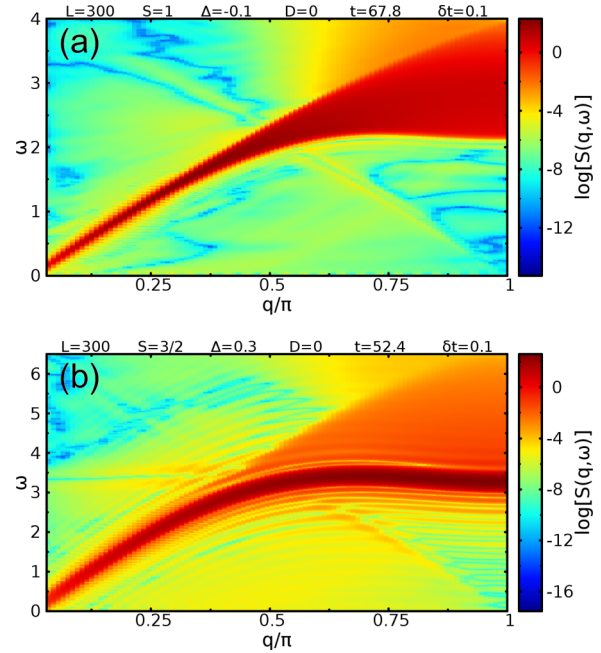

FIG. 8. The longitudinal spin structure factor of the critical spin-S XXZ chains. (a) Results for $S = 1$ and $\Delta = -0.1$ and (b) for $S = 3/2$ and $\Delta = 0.3$.

to write $\boldsymbol{\sigma}_j$ and $\boldsymbol{\tau}_j$ in terms of two fermions, say $\Psi_\sigma(j)$ and $\Psi_\tau(j)$. The resulting fermionic model turns out to be strongly interacting (and contain long-range interactions), but the low-energy sector can be treated by bosonization and a renormalization group analysis [95,97]. A critical phase with central charge $c = 1$ (analogous to the spin-1/2 XXZ model with $|\Delta| < 1$) can be understood as the result of gapping out all branches of excitations except for one remaining gapless mode.

Here, we go beyond the low-energy regime and apply the nLL theory to investigate spin autocorrelations in the critical phase of model (115). Our main goal is to test the predictions of Sec. V, namely, the frequency shift and exponential decay of oscillating terms in the boundary autocorrelation for nonintegrable models. In the bulk case, the mobile impurity model of the nLL theory can be applied phenomenologically [46] after identifying the thresholds of the spectrum in dynamical spin structure factors. Unlike the spin-1/2 XXZ model, however, the coupling between the impurity and the low-energy modes is not known exactly and is regarded as a phenomenological parameter.

As our first attempt of studying higher-S spin chains, we calculated the longitudinal spin structure factor for the model above with $D = 0$ for $S = 1$ and 3/2. The results for two representative values of Δ are shown in Fig. 8. For both values of S we notice a nearly dispersionless threshold in the spectral weight for $q \approx \pi$. This behavior is characteristic of finite-energy excitations with a large effective mass, which hinder the direct application of our theory since they introduce a small band curvature energy scale.

Focusing on $S = 1$ chains, we proceed by modifying the parameters in Eq. (115) so as to look for a regime with a larger curvature of the spectrum near $q = \pi$. Remarkably, the gap in the spectrum of $S^\parallel(q \approx \pi, \omega)$ is consistent with the
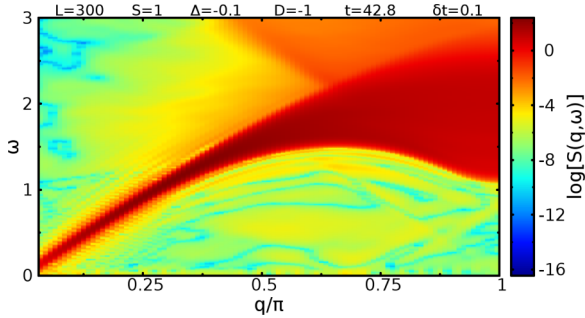
FIG. 9. The longitudinal spin structure factor of the spin-1 XXZ chain with single-ion anisotropy for $\Delta = -0.1$ and $D = -1$.

low-energy theory for critical spin-1 chains since the staggered part of the operator S_j^z excites massive modes [95,97]. We consider the model with exchange anisotropy $\Delta = -0.1$ and easy-axis single-ion anisotropy $D = -1$, which lies in the critical phase [98]. Figure 9 shows that in this case, the lower threshold of $S^{\parallel}(q,\omega)$ has a smaller gap and larger band curvature at $q = \pi$. Note also that there is no evidence for bound states in the spectrum of Fig. 9.

Next, we investigate the autocorrelation $C^{\parallel}(t,j)$ for the spin-1 chain with $\Delta = -0.1$ and $D = -1$. As discussed in Sec. V, the sharp lower threshold of $S^{\parallel}(q,\omega)$ implies that the bulk autocorrelation exhibits power-law decay of its oscillating components. Note that this argument does not depend on details of the mobile impurity model; the nonanalyticity in $C_{\text{bulk}}^{\parallel}(t)$ follows from integrating $S^{\parallel}(q,\omega)$ over momentum in the vicinity of the lower threshold. The frequencies of the oscillations can be read off from the spectrum of $S^{\parallel}(q,\omega)$ as the values of ω about which the lower threshold disperses parabolically. In the examples with spin-1/2 chains, there was only one such frequency corresponding to the band edge of single-hole excitations. By contrast, in Fig. 9, we observe two frequencies that can be identified as "edges" of the support: $W_1 \approx 1.5$ (at $q \approx 0.65\pi$) and $W_2 \approx 1.1$ (at $q \approx \pi$). Thus we have fitted the tDMRG data with the two-frequency formula

$$\text{Re}[C_{\text{bulk}}^{\parallel}(t)] = \frac{B_0^{\parallel}}{t^2} + \frac{B_1^{\parallel}\cos(W_1 t + \varphi_1)}{t^{\beta_1}} + \frac{B_2^{\parallel}\cos(W_2 t + \varphi_2)}{t^{\beta_2}}.$$

(116)

Note that in contrast with Eq. (110), here we include the nonoscillating term $\sim t^{-2}$, associated with the gapless $q = 0$ mode, but omit the term $\sim t^{-2K}$ that in the spin-1/2 case stems from $q = \pi$ part of the operator S_j^z in the LL theory. The result of the fit is shown in Fig. 10. Note that the frequencies obtained are consistent with the edges of the spectrum observed in Fig. 9.

Finally, we analyze the behavior of the boundary autocorrelation $C_{\text{end}}^{\parallel}(t)$ for the spin-1 chain with $\Delta = -0.1$ and $D = -1$. For nonintegrable models, our effective field theory predicts that boundary operators introduce a nonuniversal frequency shift and a decay rate for the high-energy mode. The numerical results indicate that the data can be fitted with a single oscillating component. We have fitted the tDMRG data for $C_{\text{end}}^{\parallel}(t)$ to two functions:

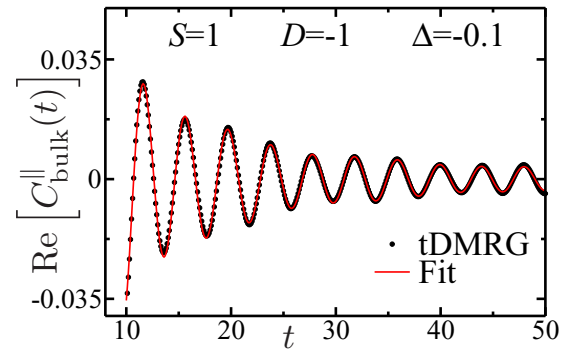$$f_1(t) = \frac{A_1}{t^2} + \frac{A_2^{\text{pl}}\cos(W't + \varphi_1)}{t^{\beta}}$$

(117)

FIG. 10. Real part of the longitudinal spin autocorrelation $C_{\text{bulk}}^{\parallel}(t)$ vs t for the spin-1 chain with $\Delta = -0.1$, $D = -1$, and $L = 300$. The data were obtained using $m = 350$ and $\delta t = 0.1$. We fit the data to Eq. (116) and obtain the frequencies $W_1 = 1.55$ and $W_2 = 1.11$ and exponents $\beta_1 = 1.57$ and $\beta_2 = 1.76$.

versus

$$f_2(t) = \frac{A_1'}{t^2} + A_2^{\text{exp}}\cos(W't + \varphi_2)e^{-\gamma t}.$$

(118)

For both fit functions we find $W' \approx 1.75$. This frequency is clearly different from the band edge frequencies W_1 and W_2 obtained from fitting the bulk autocorrelation and lies inside the continuum of $S^{\parallel}(q,\omega)$ (see Fig. 9). This result is

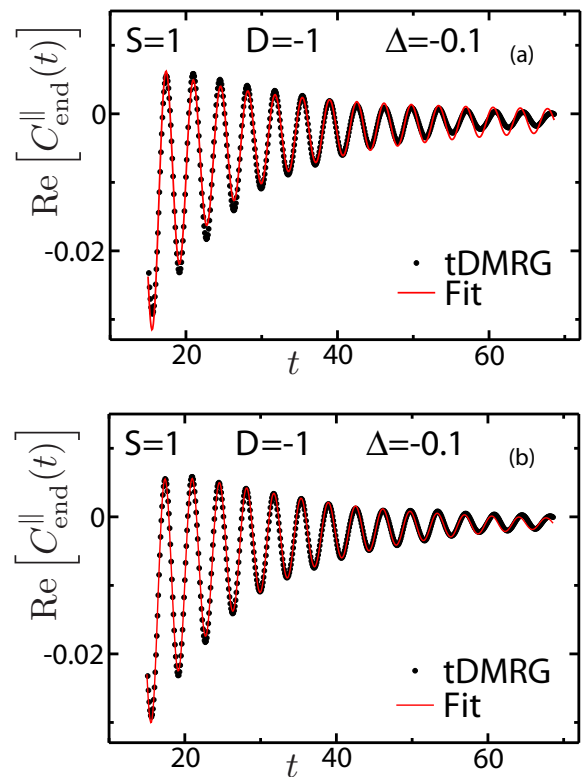
FIG. 11. Real part of the longitudinal spin autocorrelation $C_{\text{end}}^{\parallel}(t)$ vs t for the spin-1 chain with $\Delta = -0.1$, $D = -1$, and $L = 300$. The symbols are the tDMRG results. The data were obtained using $m = 350$ and $\delta t = 0.1$. (a) Fit to power-law decay in Eq. (117). (b) Fit to exponential decay in Eq. (118).
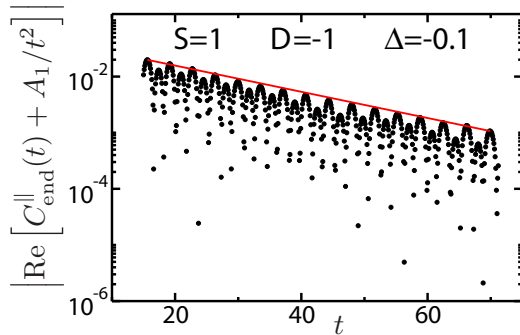
FIG. 12. Same as Fig. 11, after subtracting the nonoscillating term $\sim 1/t^2$. The prefactor $A_1 = 2.233$ was obtained independently (see Appendix). The slope of the red line is ≈ -0.053.

consistent with our prediction of a nonuniversal frequency shift for nonintegrable models. Moreover, we can see in Fig. 11(a) that the best fit to Eq. (117) for $t > 15$ overestimates the amplitude of the oscillations at larger times $t \gtrsim 45$, suggesting that the decay is faster than power law. In fact, the fit to an exponential decay according to Eq. (118) with $\gamma \approx 0.059$ yields better agreement with the numerical data [see Fig. 11(b)]. Importantly, the fitted relaxation time $1/\gamma \approx 17$ is smaller than the time scales reached by the tDMRG.

In order to observe a clear signature of the exponential decay of $C_{\text{end}}^{\parallel}(t)$, it is convenient to subtract off the nonoscillating t^{-2} term in the autocorrelation function. This subtraction is important because the difference between power-law and exponential decay of the oscillating component becomes more pronounced at longer times, after which an exponentially decaying term would become less significant than the $1/t^2$ or subleading power-law terms. As explained in Appendix, we can fix the nonuniversal prefactor A_1 in Eq. (117) by relating it to the prefactor of the uniform term in the static correlation $\langle S_1^z S_j^z \rangle \sim 1/j^2$ for $j \gg 1$. The numerical result for the boundary autocorrelation after subtracting the nonoscillating term is shown in Fig. 12. It is clear that the amplitude of the oscillations decays as a straight line on a log-linear scale. This result indicates an exponential decay of the boundary autocorrelation in the nonintegrable model, in agreement with our prediction.

VII. CONCLUSION

In conclusion, we have analyzed the effect of reflective boundary conditions in one-dimensional quantum liquids on time-dependent correlations. We have shown that one can generalize the effective impurity model of a high-energy mode interacting with the low-energy subband (nonlinear Luttinger liquid theory) to capture the dominant contributions to late-time asymptotes of autocorrelations and predict the exponents of associated power-law singularities in the frequency domain. This was used to compute, e.g., the autocorrelations in critical spin chains and the local density of states at the band bottom in one-dimensional interacting spinless fermions. The boundary exponents show a characteristic doubling in their dependence on the phase shifts, which implies relations between the bulk an boundary exponents depending only on the Luttinger

parameter but not on the phase shifts. Generalizations of the method were used to derive similar results for spinful models and different correlation functions.

Our results apply, mutatis mutandis, to the class of integrable models, but they need caution when applied to the nonintegrable case. While the impurity mode is effectively protected in the bulk by momentum conservation and power-law behavior of correlations is generic at zero temperature, the breaking of translational invariance at the boundary introduces the possibility of additional renormalization effects. We have discussed two observable consequences: a shift in the impurity energy leading to a shift in the oscillation frequency in the autocorrelation, and the possibility of decay of the impurity leading to exponential damping. These effects can be analysed within the impurity model approach by studying boundary operators as perturbations. Based on the Bethe ansatz solution for models with reflective boundary conditions, we argue that integrable models should be devoid of such effects and hence identical bulk and boundary frequencies should be observed without exponential decay.

We performed a time-dependent density matrix renormalization group study of both integrable and nonintegrable spin chains to verify our predictions. For the integrable case, we studied the XXZ spin-1/2 chain and the numerically obtained correlations agree very well with the effective field theory predictions. For the nonintegrable case, we looked at spin chains of higher spin $S > 1/2$. We did find evidence for a nonuniversal frequency shift in this case as well as an exponential damping factor of the high-energy contribution to the correlation. Detailed comparison with microscopic models highlights the properties of the spectrum one should consider in formulating the effective impurity model. First of all, one should take into account all contributions from band minima as well as band maxima. Complications may arise when the spectrum features bound states which are a priori not taken into account in the impurity model and lead to additional oscillating contributions, but the impurity model may in principle be adjusted to account for these. Bound-state lifetimes are subject to similar considerations concerning the integrable versus nonintegrable case as the high-energy impurity modes. A second complication comes when one of the high-energy bands becomes nearly flat, resulting in a very large time scale before the asymptotic behavior of the correlation is reached, which could possibly push it beyond the times for which reliable numerical data can be obtained.

An experimental test of the oscillating, high-energy contribution to correlations in real time would most likely involve the fabrication of an effective spin model using cold atom systems, for which real-space and time-resolved correlations can be imaged by many-body Ramsey interferometry [99]. To test our bulk versus boundary predictions one can resort to an optical boxlike potential [100,101] implementing the appropriate boundary condition.

It would be interesting to extend our results to more general boundary conditions. In particular, in the context of integrable models we may distinguish between integrable and nonintegrable boundary conditions. Moreover, one may differentiate between diagonal and nondiagonal boundary conditions, the latter of which corresponds to boundary conditions that do not conserve particle number in the fermionic

picture [85,102,103]. The mobile impurity model, viewed as a boundary field theory, in principle provides the flexibility to study all these situations by choosing the appropriate boundary conditions as well as adding boundary operators to account for possibly nontrivial boundary bound states.

<center>**ACKNOWLEDGMENTS**</center>

<center>**APPENDIX: BOUNDARY-BULK SPIN CORRELATION**</center>

In this Appendix, we relate the prefactors of the nonoscillating terms of the time-dependent boundary autocorrelation and of the static spin correlation. Let us first consider the critical spin-1/2 XXZ chain with open boundary conditions. We are going to show that the static spin correlation is given by

$$\left\langle S_1^z S_{j=x}^z \right\rangle \approx -\frac{2\sqrt{K}A}{\pi^2 x^2} + \frac{B(-1)^x}{x^{1+K}}, \tag{A1}$$

where K is the Luttinger parameter. The prefactor A is nonuniversal and also appears in the time-dependent boundary autocorrelation

$$\left\langle S_1^z(t) S_1^z(0) \right\rangle \sim -\frac{4A^2}{\pi^2 v^2 t^2} + \text{oscillating terms}. \tag{A2}$$

Note that if we determine the prefactor A by fitting the numerical results for the static correlation to Eq. (A1), we can fix the prefactor of the nonoscillating term in the time-dependent boundary autocorrelation.

We start with the low-energy representation for S_j^z at the boundary:

$$\begin{aligned}
S_1^z &\sim \Psi^\dagger(1)\Psi(1) \\
&\sim \ : \psi_R^\dagger(1)\psi_R(1): + : \psi_L^\dagger(1)\psi_L(1): \\
&\quad + e^{i\pi}[\psi_R^\dagger(1)\psi_L(1) + \text{H.c.}] \\
&= \ : \psi_R^\dagger(1)\psi_R(1): + : \psi_R^\dagger(-1)\psi_R(-1): \\
&\quad + [\psi_R^\dagger(1)\psi_R(-1) + \text{H.c.}] \\
&\sim 4 : \psi_R^\dagger(0)\psi_R(0): \\
&\sim -\frac{4}{\sqrt{2\pi}}\partial_x \phi_R(0).
\end{aligned} \tag{A3}$$

Next, we need to perform the Bogoliubov transformation:

$$\phi_R(x) = \frac{K^{\frac{1}{2}} + K^{\frac{1}{2}}}{2}\varphi_R(x) - \frac{K^{\frac{1}{2}} - K^{\frac{1}{2}}}{2}\varphi_R(-x). \tag{A4}$$

In the interacting case, the boundary operator has a nonuniform prefactor because the expression in Eq. (A3) mixes the staggered part of the density operator $\psi_R^\dagger \psi_L + \text{H.c.}$ (which has a nonuniversal prefactor when bosonized in the interacting case) with the uniform part $\psi_R^\dagger \psi_R + \psi_L^\dagger \psi_L$ (which does have a universal prefactor). For this reason, in the general case, we

must write

$$S_1^z \sim -\frac{4A}{\sqrt{2\pi}}\partial_x \varphi_R(0), \tag{A5}$$

where $A = 1$ for free fermions, but A is nonuniversal in the interacting case. Using Eq. (A5) together with the bosonic propagator,

$$\langle \partial_x \varphi_R(x,t) \partial_x \varphi_R(0,0) \rangle = -\frac{1}{2\pi(x-vt)^2}, \tag{A6}$$

leads to the result in Eq. (A2).

The spin operator in the bulk is given by

$$\begin{aligned}
S_{j=x}^z &\sim \Psi^\dagger(x)\Psi(x) \\
&\sim \psi_R^\dagger(x)\psi_R(x) + \psi_L^\dagger(x)\psi_L(x) \\
&\quad + (-1)^x[\psi_R^\dagger(x)\psi_L(x) + \text{H.c.}] \\
&\sim \sqrt{\frac{K}{2\pi}}[\partial_x \varphi_L(x) - \partial_x \varphi_R(x)] \\
&\quad + \frac{(-1)^x}{2\pi\eta}[e^{i\sqrt{2\pi K}[\varphi_R(x)-\varphi_L(x)]} + \text{H.c.}].
\end{aligned} \tag{A7}$$

Using the folding trick with

$$\partial_x \varphi_L(x) = -\partial_x \varphi_R(-x), \tag{A8}$$

we obtain

$$\begin{aligned}
S_j^z &\sim -\sqrt{\frac{K}{2\pi}}[\partial_x \varphi_R(x) + \partial_x \varphi_R(-x)] \\
&\quad + B'(-1)^x[e^{i\sqrt{2\pi K}[\varphi_R(-x)-\varphi_R(x)]} + \text{H.c.}],
\end{aligned} \tag{A9}$$

where B' is nonuniversal.

Let us first focus on the uniform part in Eq. (A9). The corresponding term in the static correlation is

$$\begin{aligned}
\left\langle S_1^z S_j^z \right\rangle &\sim \frac{2\sqrt{K}A}{\pi}[\langle \partial_x \varphi_R(0)\partial_x \varphi_R(x)\rangle + (x \to -x)] \\
&= -\frac{2\sqrt{K}A}{\pi^2 x^2},
\end{aligned} \tag{A10}$$

which is the first term on the rhs of Eq. (A1).

Now consider the staggered part of the operator in Eq. (A9). Since this term has a nonuniversal prefactor, which is independent of A, we shall focus on deriving the exponent of the large-distance decay. The staggered term in the correlation is

$$\left\langle S_1^z S_j^z \right\rangle \sim (-1)^x \langle \partial_x \varphi_R(0) e^{i\sqrt{2\pi K}\varphi_R(-x)} e^{-i\sqrt{2\pi K}\varphi_R(x)} \rangle. \tag{A11}$$

This is a three-point function involving three primary fields. We use the operator product expansion:

$$\begin{aligned}
&: \partial_x \varphi_R(0) :: e^{i\sqrt{2\pi K}\varphi_R(-x)} : \\
&= \sum_{n=0}^{\infty} \frac{(i\sqrt{2\pi K})^n}{n!} : \partial_x \varphi_R(0) :: [\varphi_R(-x)]^n : \\
&\sim \sum_{n=1}^{\infty} \frac{(i\sqrt{2\pi K})^n}{(n-1)!} \langle \partial_x \varphi_R(0)\varphi_R(-x)\rangle : [\varphi_R(-x)]^{n-1} : \\
&= i\sqrt{2\pi K} \langle \partial_x \varphi_R(0)\varphi_R(-x)\rangle : e^{i\sqrt{2\pi K}\varphi_R(-x)} :
\end{aligned}$$

$$= \frac{i\sqrt{K}}{\sqrt{2\pi}x} : e^{i\sqrt{2\pi K}\varphi_R(-x)} : . \tag{A12}$$

Thus, in the three-point function, we obtain

$$\langle \partial_x \varphi_R(0) e^{i\sqrt{2\pi K}\varphi_R(-x)} e^{-i\sqrt{2\pi K}\varphi_R(x)} \rangle$$

$$\sim \frac{1}{x} \langle e^{i\sqrt{2\pi K}\varphi_R(-x)} e^{-i\sqrt{2\pi K}\varphi_R(x)} \rangle$$

$$\sim \frac{1}{x} \frac{1}{(2x)^K}. \tag{A13}$$

It follows that the staggered term in the spin correlation behaves as

$$\langle S_1^z S_j^z \rangle \sim \frac{(-1)^x}{x^{1+K}}, \tag{A14}$$

which is the second term in Eq. (A1).

For the spin-1 chain, the uniform part of the spin operator in the bulk becomes

$$S_j^z \sim -\sqrt{\frac{K}{\pi}} [\partial_x \varphi_R(x) + \partial_x \varphi_R(-x)]. \tag{A15}$$

Note the extra factor of $\sqrt{2}$ in comparison with Eq. (A9), which comes from combining the densities of two spinless fermions [95] (more generally, this procedure introduces

a factor of $\sqrt{2S}$ for the spin-S operator). The Luttinger parameter in Eq. (A15) is defined such that the Kosterlitz-Thouless transition to the gapped Haldane phase happens at $K = 1$ and $K > 1$ in the critical phase [95]. Moreover, for $S = 1$, the staggered part of S_j^z couples to gapped modes (recall the spectrum is gapped at $k = \pi$). As a result, the staggered term in the static correlation decays exponentially with the distance from the boundary. The results for the autocorrelation and static correlation for $S = 1$ are

$$\langle S_1^z(t) S_1^z(0) \rangle \approx -\frac{4C^2}{\pi^2 v^2 t^2}, \tag{A16}$$

$$\langle S_1^z S_{j=x}^z \rangle \approx -\frac{2\sqrt{2K}C}{\pi^2 x^2}, \tag{A17}$$

where the coefficient C is nonuniversal. The LL parameter K and the spin velocity v can be determined independently by analyzing the finite-size corrections of the lower energy states together with the machinery of the conformal field theory [104], see, for example, Ref. [105]. We found for the spin-1 chain with $\Delta = -0.1$ and $D = -1$ the following values: $K = 1.285$ and $v = 1.211$. Using these values and fitting the DMRG data of the static correlations to Eq. (A17), we found that $C = 2.8423$.

---

[1] A. Theumann, J. Math. Phys. **8**, 2460 (1967).

[2] A. Luther and I. Peschel, Phys. Rev. B **9**, 2911 (1974).

[3] V. Meden and K. Schönhammer, Phys. Rev. B **46**, 15753 (1992).

[4] J. Voit, J. Phys. Condens. Matter **5**, 8305 (1993).

[5] T. Giamarchi, *Quantum Physics in One Dimension* (Oxford University Press, Oxford, 2004).

[6] S.-I. Tomonaga, Prog. Theor. Phys. **5**, 544 (1950).

[7] J. M. Luttinger, J. Math. Phys. **4**, 1154 (1963).

[8] K. V. Samokhin, J. Phys. Condens. Matter **10**, L533 (1998).

[9] D. N. Aristov, Phys. Rev. B **76**, 085327 (2007).

[10] S. Teber, Phys. Rev. B **76**, 045309 (2007).

[11] S. Teber, EPJB **52**, 233 (2006).

[12] T. Price and A. Lamacraft, Phys. Rev. B **90**, 241415 (2014).

[13] A. V. Rozhkov, Eur. Phys. J. B **47**, 193 (2005).

[14] M. Khodas, M. Pustilnik, A. Kamenev, and L. I. Glazman, Phys. Rev. B **76**, 155402 (2007).

[15] A. Imambekov and L. I. Glazman, Science **323**, 228 (2009).

[16] P. W. Anderson, Phys. Rev. Lett. **18**, 1049 (1967).

[17] K. D. Schotte and U. Schotte, Phys. Rev. **182**, 479 (1969).

[18] J. M. P. Carmelo and P. D. Sacramento, Phys. Rev. B **68**, 085104 (2003).

[19] R. G. Pereira, J. Sirker, J.-S. Caux, R. Hagemans, J. M. Maillet, S. R. White, and I. Affleck, Phys. Rev. Lett. **96**, 257202 (2006).

[20] M. Pustilnik, M. Khodas, A. Kamenev, and L. I. Glazman, Phys. Rev. Lett. **96**, 196405 (2006).

[21] M. Khodas, M. Pustilnik, A. Kamenev, and L. I. Glazman, Phys. Rev. Lett. **99**, 110405 (2007).

[22] R. G. Pereira, S. R. White, and I. Affleck, Phys. Rev. Lett. **100**, 027206 (2008).

[23] V. V. Cheianov and M. Pustilnik, Phys. Rev. Lett. **100**, 126403 (2008).

[24] R. G. Pereira, S. R. White, and I. Affleck, Phys. Rev. B **79**, 165113 (2009).

[25] A. Imambekov and L. I. Glazman, Phys. Rev. Lett. **102**, 126405 (2009).

[26] F. H. L. Essler, Phys. Rev. B **81**, 205120 (2010).

[27] T. L. Schmidt, A. Imambekov, and L. I. Glazman, Phys. Rev. B **82**, 245104 (2010).

[28] T. L. Schmidt, A. Imambekov, and L. I. Glazman, Phys. Rev. Lett. **104**, 116403 (2010).

[29] R. G. Pereira, K. Penc, S. R. White, P. D. Sacramento, and J. M. P. Carmelo, Phys. Rev. B **85**, 165132 (2012).

[30] P. Debray, V. N. Zverev, V. Gurevich, R. Klesse, and R. S. Newrock, Semicond. Sci. Technol. **17**, R21 (2002).

[31] M. Yamamoto, M. Stopa, Y. Tokura, Y. Hirayama, and S. Tarucha, Physica E **12**, 726 (2002).

[32] M. Pustilnik, E. G. Mishchenko, L. I. Glazman, and A. V. Andreev, Phys. Rev. Lett. **91**, 126805 (2003).

[33] D. Laroche, G. Gervais, M. P. Lilly, and J. L. Reno, Nat. Nano **6**, 793 (2011).

[34] R. G. Pereira and E. Sela, Phys. Rev. B **82**, 115324 (2010).

[35] K. A. Matveev and A. Furusaki, Phys. Rev. Lett. **111**, 256401 (2013).

[36] I. V. Protopopov, D. B. Gutman, and A. D. Mirlin, Phys. Rev. B **90**, 125113 (2014).

[37] I. V. Protopopov, D. B. Gutman, M. Oldenburg, and A. D. Mirlin, Phys. Rev. B **89**, 161104 (2014).

[38] J. Lin, K. A. Matveev, and M. Pustilnik, Phys. Rev. Lett. **110**, 016401 (2013).

[39] G. Barak, H. Steinberg, L. N. Pfeiffer, K. W. West, L. Glazman, F. von Oppen, and A. Yacoby, Nat. Phys. **6**, 489 (2010).

[40] E. Bettelheim and L. Glazman, Phys. Rev. Lett. **109**, 260602 (2012).

[41] E. Bettelheim, A. G. Abanov, and P. Wiegmann, Phys. Rev. Lett. **97**, 246402 (2006).

[42] I. V. Protopopov, D. B. Gutman, P. Schmitteckert, and A. D. Mirlin, Phys. Rev. B **87**, 045112 (2013).

[43] R. G. Pereira, Int. J. Mod. Phys. B **26**, 1244008 (2012).

[44] C. Karrasch, R. G. Pereira, and J. Sirker, New J. Phys. **17**, 103003 (2015).

[45] L. Seabra, F. H. L. Essler, F. Pollmann, I. Schneider, and T. Veness, Phys. Rev. B **90**, 245127 (2014).

[46] A. Imambekov, T. L. Schmidt, and L. I. Glazman, Rev. Mod. Phys. **84**, 1253 (2012).

[47] J. L. Cardy, Nucl. Phys. B **324**, 581 (1989).

[48] I. Affleck and A. W. W. Ludwig, J. Phys. A: Math. Gen. **27**, 5375 (1994).

[49] P. Fendley, F. Lesage, and H. Saleur, J. Stat. Phys. **85**, 211 (1996).

[50] C. L. Kane and M. P. A. Fisher, Phys. Rev. B **46**, 15233 (1992).

[51] E. Wong and I. Affleck, Nucl. Phys. B **417**, 403 (1994).

[52] M. Fabrizio and A. O. Gogolin, Phys. Rev. B **51**, 17827 (1995).

[53] S. Eggert and I. Affleck, Phys. Rev. B **46**, 10866 (1992).

[54] R. Egger and H. Grabert, Phys. Rev. Lett. **75**, 3505 (1995).

[55] A. Leclair, F. Lesage, and H. Saleur, Phys. Rev. B **54**, 13597 (1996).

[56] S. Rommer and S. Eggert, Phys. Rev. B **62**, 4370 (2000).

[57] N. Laflorencie, E. S. Sørensen, M.-S. Chang, and I. Affleck, Phys. Rev. Lett. **96**, 100603 (2006).

[58] L. Taddia, J. C. Xavier, F. C. Alcaraz, and G. Sierra, Phys. Rev. B **88**, 075112 (2013).

[59] K. Schönhammer, V. Meden, W. Metzner, U. Schollwöck, and O. Gunnarsson, Phys. Rev. B **61**, 4393 (2000).

[60] V. Meden, W. Metzner, U. Schollwöck, O. Schneider, T. Stauber, and K. Schönhammer, Eur. Phys. J. B **16**, 631 (2000).

[61] U. Schollwöck, V. Meden, W. Metzner, and K. Schönhammer, Prog. Theor. Phys. Supplement **145**, 312 (2002).

[62] V. Meden, W. Metzner, U. Schollwöck, and K. Schönhammer, Phys. Rev. B **65**, 045318 (2002).

[63] S. Andergassen, T. Enss, V. Meden, W. Metzner, U. Schollwöck, and K. Schönhammer, Phys. Rev. B **70**, 075102 (2004).

[64] S. Andergassen, T. Enss, V. Meden, W. Metzner, U. Schollwöck, and K. Schönhammer, Phys. Rev. B **73**, 045125 (2006).

[65] I. Schneider, A. Struck, M. Bortz, and S. Eggert, Phys. Rev. Lett. **101**, 206401 (2008).

[66] D. Schuricht, S. Andergassen, and V. Meden, J. Phys. Condens. Matter **25**, 014003 (2013).

[67] S. A. Söffing, I. Schneider, and S. Eggert, EPL (Europhys. Lett.) **101**, 56006 (2013).

[68] E. Jeckelmann, J. Phys. Condens. Matter **25**, 014002 (2013).

[69] S. Eggert, H. Johannesson, and A. Mattsson, Phys. Rev. Lett. **76**, 1505 (1996).

[70] A. E. Mattsson, S. Eggert, and H. Johannesson, Phys. Rev. B **56**, 15615 (1997).

[71] Y. Wang, J. Voit, and F.-C. Pu, Phys. Rev. B **54**, 8491 (1996).

[72] M. Bockrath, D. H. Cobden, J. Lu, A. G. Rinzler, R. E. Smalley, L. Balents, and P. L. McEuen, Nature (London) **397**, 598 (1999).

[73] C. Blumenstein, J. Schäfer, S. Mietke, S. Meyer, A. Dollinger, M. Lochner, X. Y. Cui, L. Patthey, R. Matzdorf, and R. Claessen, Nat. Phys. **7**, 776 (2011).

[74] S. R. White and A. E. Feiguin, Phys. Rev. Lett. **93**, 076401 (2004).

[75] U. Schollwöck, Ann. Phys. **326**, 96 (2011).

[76] E. H. Lieb and D. W. Robinson, Comm. Math. Phys. **28**, 251 (1972).

[77] C. Karrasch, J. E. Moore, and F. Heidrich-Meisner, Phys. Rev. B **89**, 075139 (2014).

[78] V. E. Korepin, N. M. Bogoliubov, and A. G. Izergin, *Quantum Inverse Scattering Method and Correlation Functions* (Cambridge University Press, Cambridge, 1993).

[79] A. Imambekov and L. I. Glazman, Phys. Rev. Lett. **100**, 206805 (2008).

[80] S. Katsura, T. Horiguchi, and M. Suzuki, Physica **46**, 67 (1970).

[81] J. Stolze, A. Nöppert, and G. Müller, Phys. Rev. B **52**, 4319 (1995).

[82] H. Karimi and I. Affleck, Phys. Rev. B **84**, 174420 (2011).

[83] F. H. L. Essler, R. G. Pereira, and I. Schneider, Phys. Rev. B **91**, 245150 (2015).

[84] F. C. Alcaraz, M. N. Barber, M. T. Batchelor, R. J. Baxter, and G. R. W. Quispel, J. Phys. A: Math. Gen. **20**, 6397 (1987).

[85] E. K. Sklyanin, J. Phys. A: Math. Gen. **21**, 2375 (1988).

[86] H. Schulz, J. Phys C: Solid State Phys. **18**, 581 (1985).

[87] L. Balents, Phys. Rev. B **61**, 4429 (2000).

[88] H. Bethe and W. Heitler, Proc. R. Soc. Lond. A **146**, 83 (1934).

[89] L. Landau and G. Rumer, Proc. R. Soc. Lond. A **166**, 213 (1938).

[90] A. Zvyagin, *Finite Size Effects in Correlated Electron Models: Exact Results* (World Scientific, Singapore, 2005).

[91] A. J. Daley, C. Kollath, U. Schollwöck, and G. Vidal, J. Stat. Mech. Theor. Exp. (2004) P04005.

[92] A. E. Feiguin and S. R. White, Phys. Rev. B **72**, 020404 (2005).

[93] F. Haldane, Phys. Lett. A **93**, 464 (1983).

[94] F. D. M. Haldane, Phys. Rev. Lett. **50**, 1153 (1983).

[95] H. J. Schulz, Phys. Rev. B **34**, 6372 (1986).

[96] F. C. Alcaraz and A. Moreo, Phys. Rev. B **46**, 2896 (1992).

[97] J. Timonen and A. Luther, J. Phys. C **18**, 1439 (1985).

[98] W. Chen, K. Hida, and B. C. Sanctuary, Phys. Rev. B **67**, 104401 (2003).

[99] M. Knap, A. Kantian, T. Giamarchi, I. Bloch, M. D. Lukin, and E. Demler, Phys. Rev. Lett. **111**, 147205 (2013).

[100] A. L. Gaunt, T. F. Schmidutz, I. Gotlibovych, R. P. Smith, and Z. Hadzibabic, Phys. Rev. Lett. **110**, 200406 (2013).

[101] L. Chomaz, L. Corman, T. Bienaimé, C. Weitenberg, S. Nascimbène, and J. Dalibard, Nat. Commun. **6**, 6162 (2015).

[102] S. Ghoshal and A. Zamolodchikov, Int. J. Mod. Phys. A **09**, 3841 (1994).

[103] X. Zhang, Y.-Y. Li, J. Cao, W.-L. Yang, K. Shi, and Y. Wang, Nucl. Phys. B **893**, 70 (2015).

[104] P. DiFrancesco, P. Mathieu, and D. Sénéchal, *Conformal Field Theory* (Springer, Berlin, 1997).

[105] J. C. Xavier, Phys. Rev. B **81**, 224404 (2010).